Thermal-hydraulic analysis of superconducting cables for energy applications with a novel open object-oriented software: OPENSC2

Cryogenics 124 (2022) 103457

Contents lists available at ScienceDirect

Cryogenics

journal homepage: www.elsevier.com/locate/cryogenics

Thermal-hydraulic analysis of superconducting cables for energy applications with a novel open object-oriented software: OPENSC^2

Laura Savoldi *, Daniele Placido, Sofia Viarengo

MAHTEP Group, Dipartimento Energia "Galileo Ferraris", Politecnico di Torino, Torino, Italy

ARTICLE INFO

Keywords:
Numerical modelling
Object-oriented model
Open-source software
Test-driven development
Thermal-hydraulic transients
Superconducting cables for energy applications

ABSTRACT

Super-conducting cables are an enabling technology for energy applications such as large magnetic-confinement nuclear fusion machine, and a promising key player in the power transmission of the next future, both in AC and DC conditions. While the thermal–hydraulic analysis of forced-flow superconducting cables for fusion application can only rely on commercial or proprietary numerical tools, such kind of tools for power transmission cables are not even available. Within the framework of Open Science, set as a priority by the European Commission in Horizon Europe, the novel software **O**PEN **S**uper **C**onducting **C**ables (OPENSC^2) has been developed to grant the entire research community the possibility to simulate thermal–hydraulic transients in forced-flow superconducting cables for energy applications. A Test-Driven Development has been adopted for the OPENSC^2 within an object-oriented approach. Following the TDD approach, three test cases are considered of paramount interest for the OPENSC^2 development, deriving the set of characteristics that the target object-oriented tool should comply with, and namely: 1) a heat slug propagation along an ITER-like 2-region cable-in-conduit conductor, with a thousand of mm-size low-critical-temperature superconducting (LTS) strands, cooled by supercritical helium (SHe); 2) the heat diffusion across the cross section of a twisted-slotted-core cable-in-conduit conductor, with high-critical-temperature (HTS) superconducting tapes, for fusion application, cooled by SHe and 3) the nominal operation of a single-phase HTS High-voltage, Direct Current power cable, with a 2-cryostat configuration and 2 different fluids adopted as primary coolant and thermal shield. In the object-oriented OPENSC^2 the class "conductor" is defined, where each Conductor Object (CO) is the combination of different lower-level objects (both fluid and solid components) instantiated by the class. The choice of each component drives the automatic selection of the appropriate physical equation(s) in the code, as well as the possible interactions between them. Thermo-physical properties of different materials and cryogens can be attributed to the components of a conductor objects, taken form open datasets. A user-friendly GUI allows setting and monitoring the simulations while running. The software is tested in the three case studies targeted in the TDD, to show eventually how it allows modeling the three test cases presented here. The Verification and Validation of the CO methods performed through benchmarks against the 4C code is also presented and discussed.

1. Introduction

1.1. Background

Superconducting (SC) cables and magnets in the past decades have enabled fundamental discoveries in the field of high-energy physics [1], amazing steps forward in the research on a clean energy based on nuclear fusion [2] and a significant increase in the power transfer capability, as well as reduction of transmission loss and construction cost, for power cables [3]. Also in medical applications, they have allowed reaching remarkably high magnetic fields in the most advanced Nuclear Magnetic Resonance spectroscopy and magnetic resonance imaging [4]. Among the electric power applications [5], they entered the sector of generation, transmission and improvement of the electric grid quality with, for instance, SC motors, Fault Current Limiter (FCL), synchronous condensers and the Superconducting Magnetic Energy Storage (SMES) [6]. Diverse kinds of SC cables are available, according to the applications, based on different SC materials and different concepts of cooling (conduction-cooling, coolant bath or forced-flow): we concentrate here on forced-flow SC cables.

* Corresponding author.
E-mail address: laura.savoldi@polito.it (L. Savoldi).

https://doi.org/10.1016/j.cryogenics.2022.103457
Received 17 December 2021; Received in revised form 12 March 2022; Accepted 3 April 2022
Available online 9 April 2022

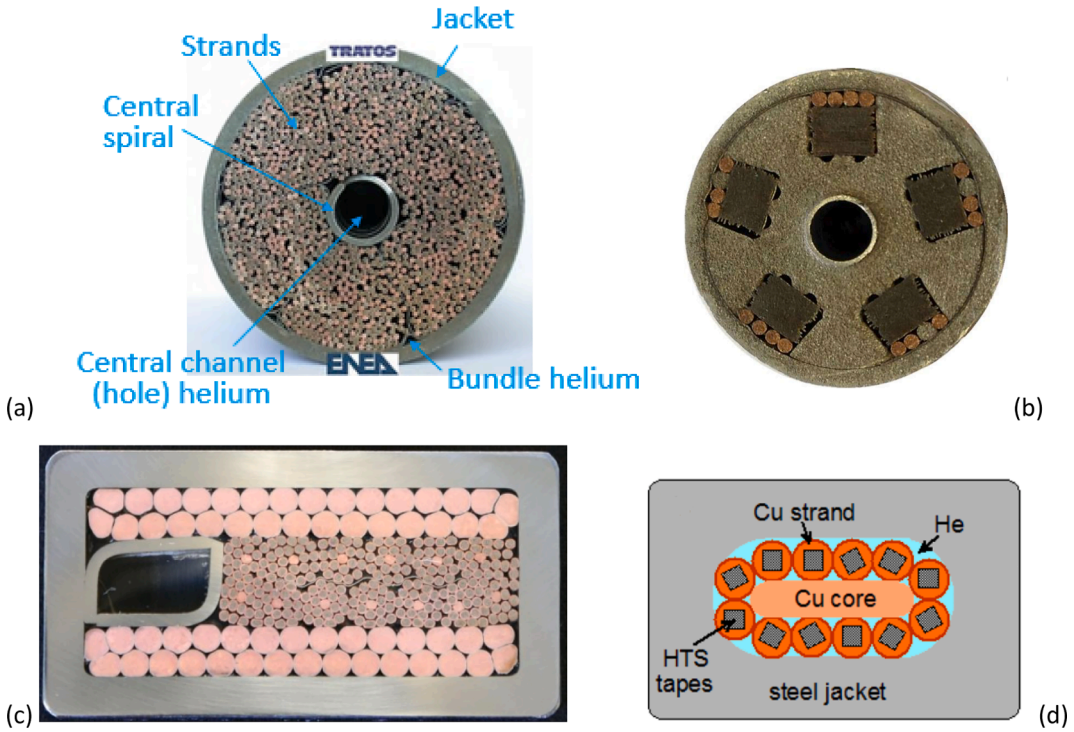

Fig. 1. Different examples of LTS and HTS cables for fusion applications: (a) Nb_3Sn ITER-like cable (courtesy of ENEA); (b) HTS slotted-core cable (courtesy of ENEA); (c) LTS CICC proposed for the EU-DEMO Toroidal Field Coils (courtesy of the Swiss Plasma Center); (d) HTS Rutherford-like cable (Swiss Plasma Center design).

High-Energy Physics (HEP) magnets use high-current, multi-strand superconducting cables [7] to reduce the number of turns in the coils, reducing then the magnet inductance. Typically, the HEP coils are wound using Rutherford cables, developed already in the early 1970s and particularly suitable for that kind of magnets due to their excellent mechanical, electrical and thermal properties. Rutherford cables, widely used in NbTi and Nb_3Sn magnets, are typically conduction-cooled, and their modeling is beyond the scope of the present paper. Other designs are being developed, such as the tilted solenoids, based also on High-Critical Temperature superconductors (HTS), opening the opportunities to continue advancements toward higher magnetic fields, but also to operate at an increased temperature [8]. However, also the HTS coils for HEP typically rely on conduction cooling through the device, cooled on the outer side natural convection to a 2-phase cryogen fluid.

The research on nuclear fusion as a possible technology for a CO_2-free power production, capable to reduce the many issues related to the nuclear fission plants [9,10] is flourishing around the world, with magnetic confinement devices being designed or constructed, by both public enterprises and private companies, to address the physics and technological challenges that are still open. Despite the alternative configuration and design choices, all the large fusion machine recently entered in operation, under commissioning or design are superconductive.

On the side of the stellarator/heliotron configuration, the two world largest operating machines, and namely Wendelstein 7-X [11–13] in Germany and the Large Helical Device in Japan [14,15], relies on superconducting coils employing Low Critical Temperature Superconducting material (LTS), cooled by Helium, mainly in forced flow conditions [16]. Future machines, such as that targeted by the public consortium EUROfusion (namely, the HELIcal Advanced Stellarator - HELIAS machine [17]) or by the private company Reinassance Fusion [18], will be designed taking advantage of the recent development in both LTS and HTS, respectively [19].

On the side of the tokamak configuration, while the ITER machine [20,21] is under construction in France, the main parties collaborating for that huge nuclear fusion experiment are separately working on the next step toward a commercial use of fusion power [22]. The China Fusion Engineering Test Reactor (CFETR) [23,24], designed to bridge the fusion experiments between ITER and a nuclear fusion power station, addresses steady-state operation and tritium self-sustainment. At the end of the conceptual design phase, its design currently relies on both LTS and HTS cable-in-conduit conductors (CICC) [25]. The European DEMOnstration reactor, in the European roadmap to fusion [26], should go beyond ITER and show for the first time that electricity can be generated from the fusion process. The EU-DEMO has just finished its pre-conceptual design phase, and its magnetic system is based on the use of CICC, with different variants still open including both LTS and hybrid LTS / HTS coils [27]. The Japanese DEMO JA-DEMO [28] is also designed as a superconducting machine, and relies on the technical maturity of the LTS Nb_3Sn technology as the prime superconductor (SC) option, at least for the Toroidal Field Coils. The design of the magnet system of the Korean DEMO K-DEMO [29] is based on the use of well-established Nb_3Sn and NbTi CICC [30]; while the American pilot power plant, ARC [31], bets on the development of fusion-class HTS magnets with a demountable structure [32], that should be already adopted in the wingdings of the SPARC (Short Pulse Affordable Robust Compact) machine [33], coming first (and soon) in the American accelerated pathway to fusion energy. Even the “satellite” tokamaks, which should complement the physics advancement reachable through the deployment of ITER within a “broader approach” to fusion energy [34], such as the JT-60SA and the Italian Divertor Tokamak Test (DTT) facility [35] are or will be fully superconductive. The JT-60SA, starting operation in Japan [36], uses LTS CICC for all the coils [37], while for the DTT, HTS cables are being considered as an insert to the Central Solenoid [38]. An overview of some of the common topologies of LTS and HTS cables for fusion applications are reported in Fig. 1. In all cases the capability of modeling of the thermal–hydraulic transients is mandatory for the design and operation of the magnets.

Superconducting cables are also currently under investigations to substitute or retrofit standard conductors in the power transmission,

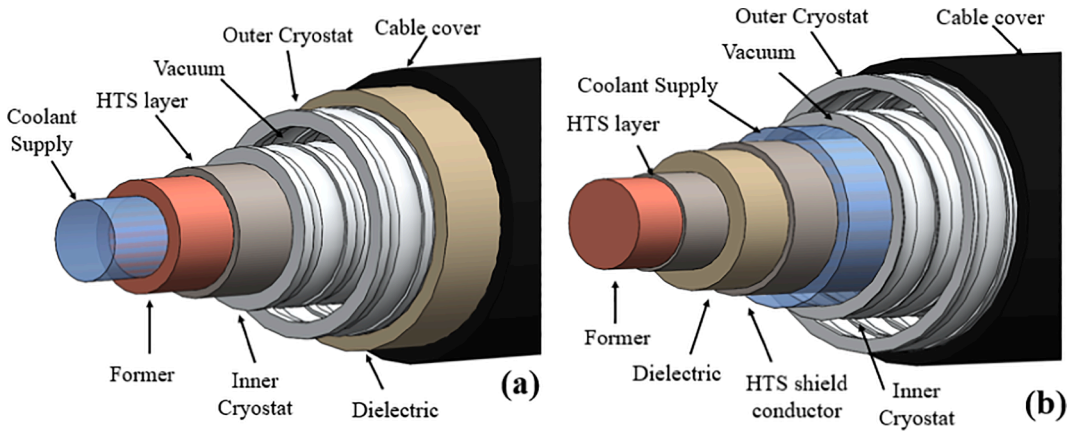

Fig. 2. Sketch of HTS DC cables with warm (a) and cold (b) dielectric, respectively.

both in AC and DC conditions. HTS AC and DC transmission cables and lines could bring a clear size advantage and low total electrical losses for high-capacity transmission, having the potential to address the need for more sustainable and efficient transmission, compared to solutions based on standard conductors [39]. Several utilities around the world have already demonstrated the technical feasibility of SC cables for power transmission, [40–43], but the technology is far from being commercial. The Superconducting transmission cables (SCTCs) are typically characterized by a transverse dimension of few tens of centimeters, with a characteristic length of the cables larger than the transverse dimension by several order of magnitude. Many different cable designs for SCTCs have been developed so far, see for instance the cold-dielectric and the warm-dielectric design reported in Fig. 2, or the single core or multiple cores for the three-phases designs in [44]. Notwithstanding the adopted design, however, the global design of Superconducting transmission lines requires a thermal–hydraulic assessment, because of the use of pressurized coolant and the need for refrigeration or compression stations along the line.

1.2. State of the art in the thermal–hydraulic modeling of HTS and LTS SC cables

Being the use of forced-flow SC cables so relevant both for fusion applications and for power transmission, the availability of an appropriate, reliable and flexible modeling of the forced-flow SC cables is of paramount importance. While the European Community is strongly supporting Open Science, set as a priority by the European Commission in its program Horizon [45], the software accepted and commonly used for the thermal–hydraulic analysis of LTS and HTS cables for fusion, which is supported in Europe by public funding, are not publicly available.

Several numerical tools are well established for the analysis of the transients in LTS cables for fusion, and namely the THEA/SUPERMAGNET Suite [46], the VINCENTA/VENICIA suite [47] and the 4C code [48]. The code THEA/SUPERMAGNET is a commercial code, of which the source files are made available upon license payment. It is based on the Gandalf code [49], originally developed for LTS CICC, and it can perform steady and transient Thermal, Hydraulic and Electric Analyses (THEA) of forced-flow SC cables. The model solves 1D mass, momentum and energy conservation for the coolant (SHe and N_2 in single phase) in the non-conservative variable velocity, pressure and temperature, and energy conservation for the solid elements along each cable. An arbitrary number of thermal and hydraulic components can be mutually coupled on the cable cross-section, with different possible materials forming the cable (SC, stabilizer, insulator, …) and variable cross sections along the cable to account for joints. The model solver uses Finite Elements Method (FEM) in space, with an adaptive grid and an adaptive multi-step time marching scheme, with an accuracy up to the 3rd order. Although a post-processor is available within the tool, no interactive simulations are possible. The code has already been applied to the modeling/design of HTS magnets or inserts in the fusion field [50]. Note, however, that the applicability of models that cannot accurately account for transversal temperature gradients across the HTS strand cross section are currently under discussion [51]. The code structure is declared as “open”, upon payment of the license fee.

VINCENTA/VENECIA is another commercial package, aimed at the transient thermal–hydraulic simulation of large SC magnet system and accounting for several coolants simultaneously: Helium, in the different states (superfluid, supercritical, or 2-phase homogeneous mixture), but also Nitrogen, Hydrogen, Oxygen, Neon and Water. The code is applicable to a wide range of devices including not only fusion ones, for which a validation of the code against experimental results is provided, but also magnet systems for NMR and MRI and superconducting motors, generators and SMES. It is based on a modular structure, with an individual set of algebraic equations, differential equations and equations in partial derivatives describing each component of the system (SC cables, pumps, valves and heat exchangers, …). Fluid flows are modeled using a 1-D approximation, solving conservation laws in the variables velocity, pressure and enthalpy, and they can be connected each-other and to 2D models of the solid elements. The spatial discretization of the derivatives is performed through Finite Differences Method (FDM) with accuracy up to 5th order, while a semi-explicit splitting-up scheme for parabolic partial differential equations is implemented for the time marching. When different conductors are modeled, each conductor can have a different meshing to better capture regions where the gradients of the drivers/solutions could be steep. Real-time monitoring of the results is included in the software, with also a GUI allowing for the selection of the task directory, of input file, visualization of 2D mesh for the solids, launch of simulation, selection and plotting of results.

Among the numerical tools mentioned above, the 4C code, which is proprietary and not available for commercial use, is largely the most validated among the ones quoted above. It can perform steady and transient Thermal-Hydraulic analyses of He-cooled forced-flow SC cables and magnets. The tool consists of different modules (one for the SC cables and winding pack, one for the bulky structures and one for the cooling circuit), suitably coupled and synchronized by a co-simulation commercial platform. The 4C module for the SC conductors and winding packs is the only one of interest here. It is inherited from the Multiconductor Mithrandir (M&M) [52], and consists of a multiconductor model for the simulation of thermal–hydraulic transients in SC winding packs wound with CICCs. 1D mass, momentum and energy conservation, are solved as in Gandalf for the coolant (Supercritical He, SHe). Transient heat diffusion is solved separately for the strands and the jacket (see Fig. 1 for the nomenclature). The possibility of a slow

variation of coolant and solid cross sections along the cables was introduced several years ago in the code to account for the peculiar topology of joints [53], but was seldom used throughout the years. As far as the numerical aspects are concerned, the 4C module under analysis uses 1st order FEM for the spatial discretization with an adaptive grid, and an implicit (Backward Euler) or semi-implicit scheme for the time marching, with an accuracy up to the 2nd order and the possibility to adapt the time stepping to capture steep variation in the cable transients. The thermal coupling between neighboring conductors within the winding pack is considered with an explicit algorithm, that at any time step quantifies the power exchange from between conductors based on the temperatures computed at the previous time step. The code is not equipped with any GUI: the post-processing is typically performed *a posteriori* using a different software (MATLAB, Excel, …). The code has been originally developed for LTS cables, however a model for HTS cables (H4C,) has been recently added to the 4C code family, which allows easily to model HTS macro-strands such as those shown in Fig. 1. d, and it is currently under validation. However, it is not suited for ITER-like LTS cables as it includes a simplified treatment for the thermal–hydraulic coupling between different cooling channels.

The three above-mentioned software have been all extensively applied in simulation for the main SC tokamaks, for "short" transients (stability and quench of conductors, for instance) and "long" transients (operating modes, cool down, warm up etc.), for both design and verification purposes of normal operating conditions [54], as well as for the investigation of off-normal operating conditions. Note that the design of different plasma scenarios for the fusion machines requires in principle the verification of the feasibility of the corresponding current scenarios in the different magnets, which can be done only relying on computational tools. Although few benchmarks are available on couples of the above-mentioned tools [55], the different codes have never been applied to the same test case and rigorously benchmarked. Furthermore, these tools are either commercial or proprietary, and cannot be freely used by the scientific community. Notwithstanding the validation path of any of the tools, their opacity rises then the issue of the verifiability of the computed results, based on which public money are allocated and invested, and that calls for a shift of paradigm towards Open Science, where an open-access tool could be used by several teams in different labs to confirm the suitability of designs and feasibility of operating scenarios.

The numerical modelling of the SCTCs is much more limited than that of the fusion cables and magnets, and it is mainly addressing the support of the cable design towards the development of a stable, reliable and safe component. A recent review of the thermal–hydraulic models for such cables showed that no numerical tools are "universally" established and available for the analysis of SCTCs, possibly in view of the variety of different topologies and cooling configurations actually under consideration for AC and DC SCTCs [44].

1.3. Modelling gaps and needs

If a wholistic approach is considered for the forced-flow SC cables modeling, the first clear point is that, notwithstanding the similarities between the cables for fusion and for power transmission, there is not a single model already available for the analysis of thermal–hydraulic transients in both kinds of cables.

Although the topology is different for the two kinds of cables, similarities exist: the SC tapes or strands are typically in contact with a stabilizer (in the form of strands, slotted core, or a former tube) and also suitably in contact, either directly or indirectly (through the stabilizer) with the coolant. The three above-mentioned components are embedded in a single or multiple jacket. The outer jacket (or insulation) is exposed to heat load either from the environment (by radiation or convection) or from other cables (by conduction within a winding pack). If field and current operation are considered for both applications, the heat source coming from AC losses is a driver for the thermal–hydraulic analysis for both cables for fusion and for power transport.

If we just remain within the fusion cables, some of the codes originally developed for the modeling of LTS cables, where the wetted perimeter of the exceedingly small strands and their large and isotropic thermal conductivity ensures the vanishing gradients inside a single strand, show issues in the modeling of fast transients such as quench propagation in the HTS cables [51]. In fact, the HTS copper-oxides tapes have a small and anisotropic thermal conductivity with respect to LTS strands, allowing for the build-up of large gradients within the single bulky strand. The HTS strands are significantly larger than the LTS ones, and the occurrence of thermal gradients in fast transients requires the modeling of each strand separately. While THEA/SUPERMAGNET can deal with that, the 4C code cannot – that was the main rationale for the development of the H4C module, which, however, is not suited for the analysis of LTS because of the explicit nature of the numerical coupling between the equations for the strands and those for the coolant.

The modeling of SCTCs per se would not require a tool capable to deal with transverse heat transfer in a winding pack, but the modeling of an entire power transmission line would require the capability to deal with an external cryogenic circuit, re-pumping stations, current leads, joints and terminations. These issues are common to the fusion applications, where the cryogenic circuit for the SC magnets must be included, if realistic operating conditions are wished for the simulations at the winding pack inlets/outlets.

Well-established tools adopted for fusion cables, as 4C for instance, at present cannot deal with SCTCs. The main missing ingredients are the capability to adopt LN_2 as coolant (included, however, in the VINCENTA/VENICIA tool), and they do not include radiative heat transfer that occurs in the cryostat(s) in the cables for power transmission, see Fig. 2. THEA/SUPERMAGNET and 4C could be possibly extended to deal with SCTCs, but the fact that they are proprietary or commercial link their extension to the interest of any stakeholders, possibly ready to cover the cost of a license (THEA/SUPERMAGNET) or development (4C). Note, however, that the two communities (the fusionist one and the transmission-cables one) do not seem to have strong connections.

As several fusion machines are under construction and are entering or will enter in operation in few years, the need for having a simulation interface that allows for the monitoring of the transient under investigation is necessary, so that a GUI allowing such monitoring is to be envisaged. Also, for the SCTCs, the monitoring of the evolution of the transient could be beneficial in the design phase to early identify in the simulation the onset of fault conditions.

1.4. Aim of the work and challenges for a novel software

Based on the above state-of-the-art in the modeling of LTS and HTS cables for fusion and power transmission, and on the gaps and needs for their modeling with a wholistic approach, the main challenges that the novel numerical tool should address, aiming at the modeling in an open framework of thermal–hydraulic transients in the different kinds of cables, are:

- Flexibility in the modeling of quite different cable structures, which can be achieved through an object-oriented development of the model, based on a basic pool of test-cases that the model should be able to deal with.
- Flexibility in the modeling of the cable coolants, which can be again achieved through an object-oriented development of the model, allowing the choice of the coolant for any of the hydraulic channels considered in the model. Such flexibility calls for an efficient implementation of the thermophysical properties of various kinds of coolant, or an efficient link to open-source libraries for that, and a suitable selection of the conservation equations describing the coolant thermal–hydraulic transient.

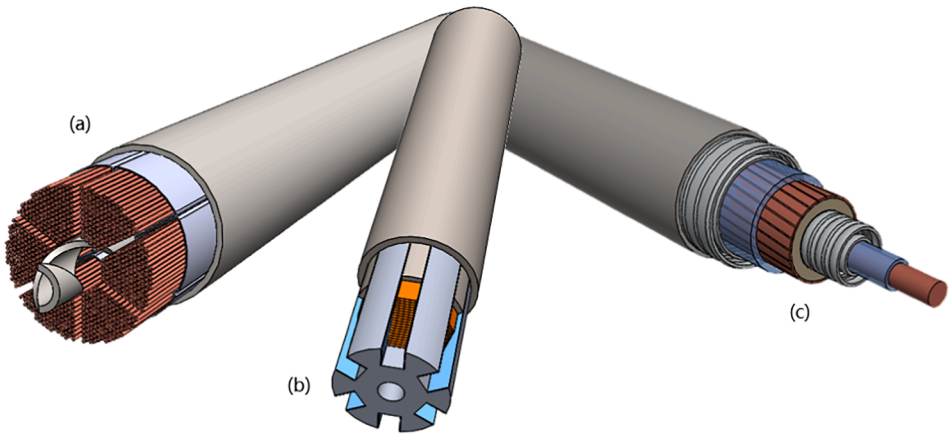

Fig. 3. Sketch of the layout of different SC cables used for the TDD: (a) ITER-like LTS cable for fusion; (b) ENEA design for HTS slotted-core cable for fusion; (c) single-core HTS cable at high-voltage in direct current (HVDC) for power transmission.

Table 1
Test 1: geometrical and operation attributes of the selected ITER TF-like conductor.

Parameter	Unit	Value
Conductor length	m	10
Strand cross section	m^2	7.54×10^{-4}
Strand material	–	Nb_3Sn (32.4%), Cu (67.6%)
Inclination angle θ of strands wrt conductor axis	–	$\cos\theta = 0.97$
Jacket cross section	m^2	5.87×10^{-4}
Jacket material	–	Stainless Steel (52.3%), GE (47.7%)
Bundle channel cross section	m^2	3.7×10^{-4}
Bundle channel fluid	–	SHe
Bundle channel hydraulic diameter	m	3.27×10^{-4}
Central channel cross section	m^2	5.03×10^{-5}
Central channel fluid	–	SHe
Central channel hydraulic diameter	m	8.00×10^{-3}
Coordinate of heated length (begin – end)	m	1 – 3
Deposited power density	W/m	250
Heating duration	s	10
Heated component	–	Strand

- Inclusion of all different mechanisms for heat transfer to the jacket and among different jackets, including not only conduction, but also convection and radiation.
- An efficient GUI, allowing the monitoring of the evolution of selected variable throughout the transient (by means of real-time plots), and ready to comply with the possibility of exploring possible control strategies and mitigation techniques as the simulation is evolving.

The object-oriented nature of the novel tool calls for a development environment suitable for that, for instance Python, a high-level interpreted and complete scripting language developed in the late 1980s. The choice of Python 3 as programming language (Python 2 is no longer maintained) is related to its popularity and to its open-source essence guaranteed by the Python Software Foundation License Agreement, its portability and simplicity, as well as its versatility ensured by the vast standard library and the availability of numerical packages that can be imported when needed from the Python Package index.

Finally, the main challenge the novel tool should address is that of transparency and accessibility, within the framework of Open Science.

The aim of the paper is to present a novel numerical tool, OPENSC^2, that addresses all the above-mentioned challenges. The development of the tool is Test-Driven: three different test cases were selected prior to the development, which cover the main modeling features the code should deal with, as explained in Section 2. The definition of the CONDUCTOR class of component, with its attributes and methods, is pursued in Section 3, together with a sketch of the user-friendly GUI developed for the OPENSC^2. Then the evidence of OPENSC^2 to pass the tests identified in Section 2 is shown, and the three selected test cases are analyzed. Test 1 also allowed to perform the code solution verification through a detailed spatial and time convergence analysis, and a benchmark against the 4C results for the same simulation setup.

2. Test-driven development of the model

For the development of OPENSC^2, a sort of light version of the Test-Driven Development [56] was applied. First, the minimum subset of case studies (cables or geometries) was identified, see Fig. 3, the TH transients of which we want to be capable to address and simulate with the novel tool. Then the different specific aspects of the physics of the case studies, that were to be captured by the code, were defined and listed. In the perspective of the TDD, the different "tests" were basically all the different functionalities the code should be able to comply with, i.e. all the different ingredients that the novel tool should be able to put together. Three different complex (non-trivial) TH transients, one per case study, were identified and the OPENSC^2 had to pass the check of capability of correctly capturing the peculiarities of the different transients.

2.1. Test 1: Heat slug propagation in an LTS conductor for fusion

The simplest topology the OPENSC^2 should be able to model is that of the classical two-regions CICC for fusion, such as that reported in Fig. 3a. A thousand strands, both superconducting (with Nb_3Sn filaments) and of segregated copper, are twisted in multi-stage twisting path around a central spiral, delimiting a low impedance channel for the coolant. The cable is encompassed in a stainless-steel jacket, providing mechanical robustness and confinement for the coolant. The jacket is typically wrapped in insulation layers (not shown in Fig. 3a). In the case at hand, the jacket is a pipe. Supercritical Helium at typically 0.6 MPa and 4.5 K is pumped through the central channel region, as well as through the space left free from the strands in the annular region. The cable transverse dimension is typically ~ 5 cm, while the length can reach several hundred of meters. Such cable can carry a current up to ~ 100 kA, in a background field up to 13 T, and works either in steady-state or in pulsed mode, bearing in the latter case significant AC losses.

The configuration in Fig. 3a, as well as similar configurations with a thicker circle-in square jackets, have been extensively investigated using the 4C code, THEA/SUPERMAGNET and VINCENTA/VENICIA [35] for the ITER coils, for a wide range of thermal–hydraulic transients ranging from the (slow) cooldown and standard plasma pulse to the fast

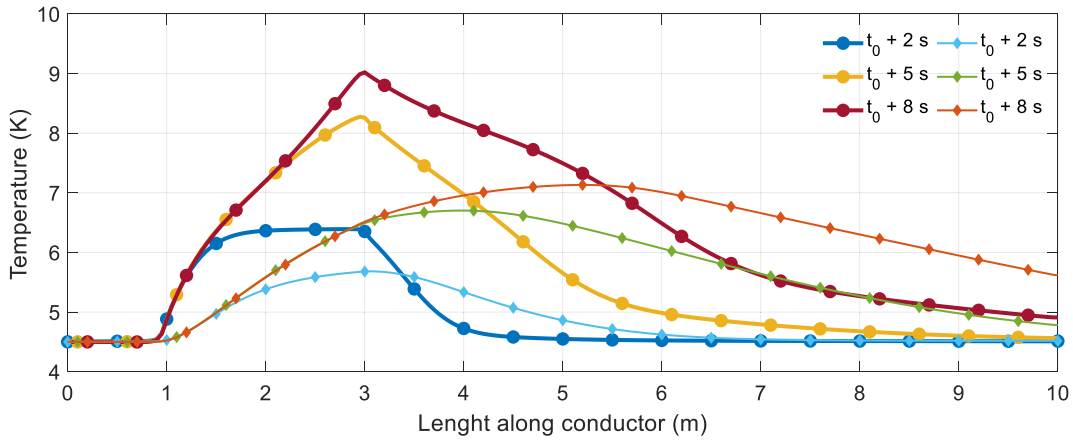

Fig. 4. Spatial profile of the temperature computed along the strands (tick solid lines with circles) and central channel (thin solid lines with diamonds) of the ITER TF-like conductor of Test 1, at a time corresponding to 2 s, 5 s and 8 s after t_0, the beginning of the square wave heating deposited in the strands.

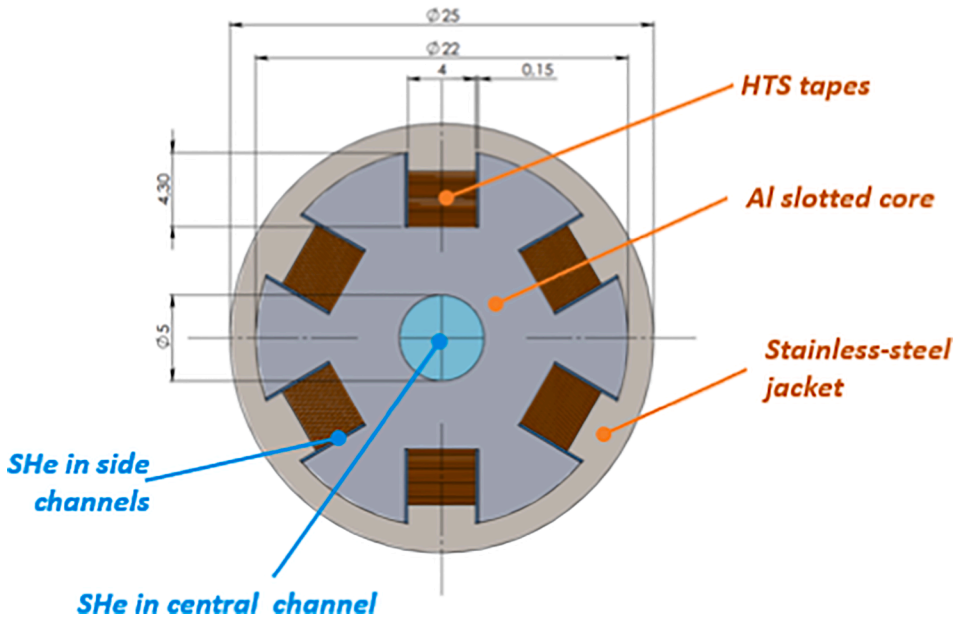

Fig. 5. Layout of the Test 2 conductor, with geometrical details (in mm).

discharge and quench. For the verification of the design of JT-60SA, KSTAR and EAST the THEA/SUPERMAGNET code has been widely used, with poor verifications performed independently with other numerical tools.

The OPENSC[2] objective for the first test case is to demonstrate the capability to correctly reproduce a thermal–hydraulic transient such as the propagation of a heat slug along the conductor in a 2-regions, ITER-type CICC. A short length of the cable (10 m) is considered in this first test, with the geometrical and operational attributes reported in Table 1. The central 2 m of the cable strands are heated with 250 W/m for 10 s, and the transient behaviour of the cable is analysed for the first 20 s after the slug begins. The test of the new tool should fail until the computed temperature evolution along the cable equals that computed by means of the 4C code. As a reference, the temperature computed using 4C along the strand and the central channels at selected times during the heating phase are reported in Fig. 4, showing the peculiar features of the trailing temperature slug in the central channel, due to the low hydraulic impedance (high speed) of the fluid in that region.

In view of the vastly different spatial scales across and along the cable, a 1D model of the different cables components has been typically adopted in most of the applications for ITER-like conductors. In general, in normal-operating transients the temperature of the entire strand bundle on the cross-section of the cable can be considered uniform and modeled by a single transient heat conduction equation. The strands are cooled by the cryogen in the bundle annular region. As far as the coolant is concerned, it has been demonstrated that the proper modeling of the heat slug propagation along the cable requires a set of 1D equations to describe the conservation of mass, momentum and energy, separately for the coolant in the central channel and in the bundle region (in the space within the strands). Each fluid region should be able to transfer mass, momentum and energy to the other one, through the central helix that offers both a permeable and impermeable interface among the two regions available for the coolant. The cryogen relevant for such application is SHe, which is highly compressible in the temperature and pressure ranges at hand. The conductor model should be completed by a 1D transient heat conduction equation for the jacket, the temperature of which is lumped in a single value for the entire cross section and can vary only along the cable.

2.2. Test 2: Heat diffusion across an HTS cable for fusion

Based on the concept of CICCs, recently a layout has been proposed

Table 2
Test 3: geometrical attributes of the selected conductor for power transmission.

Parameter	Unit	Value
Conductor length	m	100
Diameter of SC wires + stabilizer	mm	5
Inner coolant channel thickness	mm	1.5
Inner coolant		GHe
Inner cryostat – inner wall thickness	mm	2
Inner cryostat – outer wall thickness	mm	2
Insulator thickness	mm	5
Insulator material		Glass epoxy
Electric Shield thickness	mm	1
Shield material		Glass epoxy
Outer coolant channel thickness	mm	3
Outer coolant		GN_2
Outer cryostat – inner wall thickness	mm	2
Outer cryostat – outer wall thickness	mm	2
Cryostat material		Stainless Steel

for a fusion cable, based on stacks of HTS coated tapes inserted in a slotted core of a metallic stabilizer. In the design reported in Fig. 3b (which is just one of the concepts under tests, see [57]), the stacks are located in suitable helical slots available in an aluminum core, serving as stabilizer for the superconducting tapes. Metal spacers or wires (such as those in Fig. 1d, representing a similar cable) on top of the HTS stacks keep the stacks in place. The cable is insulated with a wrapping (not shown in Fig. 3b) and pulled inside the jacket, again providing mechanical robustness and confinement for the coolant. The coolant is pumped in the central channel and in the small gaps on the sides of the tape stacks in all the slots, to directly cool the HTS tapes. The transverse dimension of the cable is of few centimeters, while the relevant length for fusion applications should reach hundreds of meters. The cable could carry a current of 20 kA at 4.2 K and 15 T of background field. The coolant foreseen for this application is again SHe at 0.6 MPa and 4.5 K, mainly because the first application currently foreseen for this cable is in the winding of an insert coil for the DTT facility, and the compatibility with the cooling conditions for the LTS cables must be preserved.

The second test case identified for the OPENSC^2 development is to demonstrate the capability to correctly reproduce the propagation of a heat slug initiated in a single SC slot across (and along) a 3 m-long conductor, cooled by 5 g/s of SHe @ 4.5 K, 0.6 MPa. The heating obtained depositing 250 W/m on the central 5 cm of a single SC slot occurs for a duration of 1 s. The geometrical and material attributes of the cable are sketched in Fig. 5. The test of OPENSC^2 should fail in case of a non-symmetric slug propagation across the cable section.

As already shown in [58], the thermal–hydraulic modeling of such cable requires the capability to lump the thermal model of the slotted core (pure stabilizer) in a suitable number of 1D regions, thermally coupled by suitable fictitious thermal resistances. Each cable stack can be modeled separately or, if needed, even each of the 20 tapes within a single stack can be modelled separately as pure SC elements. The coolant modeling requires the capability to capture the mass, momentum and energy conservation in the central channel and, separately, in each of the gaps beside of the stacks. The OPENSC^2 modeling requirements for this test case are completed by the need for a transient heat conduction equation for the jacket.

2.3. Test 3: Nominal operation of an HTS cable for power transmission

An interesting cable design for High-Voltage Direct-Current (HVDC) power transmission, that could help the integration of decentralised renewable energy systems into the power grid with reduced energy losses in transportation and reduced environmental impact is shown in Fig. 3c. The cable layout is similar to that developed within the European Project BEST PATHS [59]. Moving outward, the cable is constituted by a bundle of copper wires, that serve as stabilizer to a ring of HTS wires (MgB_2 in the case of BEST PATHS), inserted into a corrugated pipe (jacket) where the primary coolant (GHe) is pumped. The jacket is part of the first cryogenic envelop: it is vacuum separated by a spacer from a

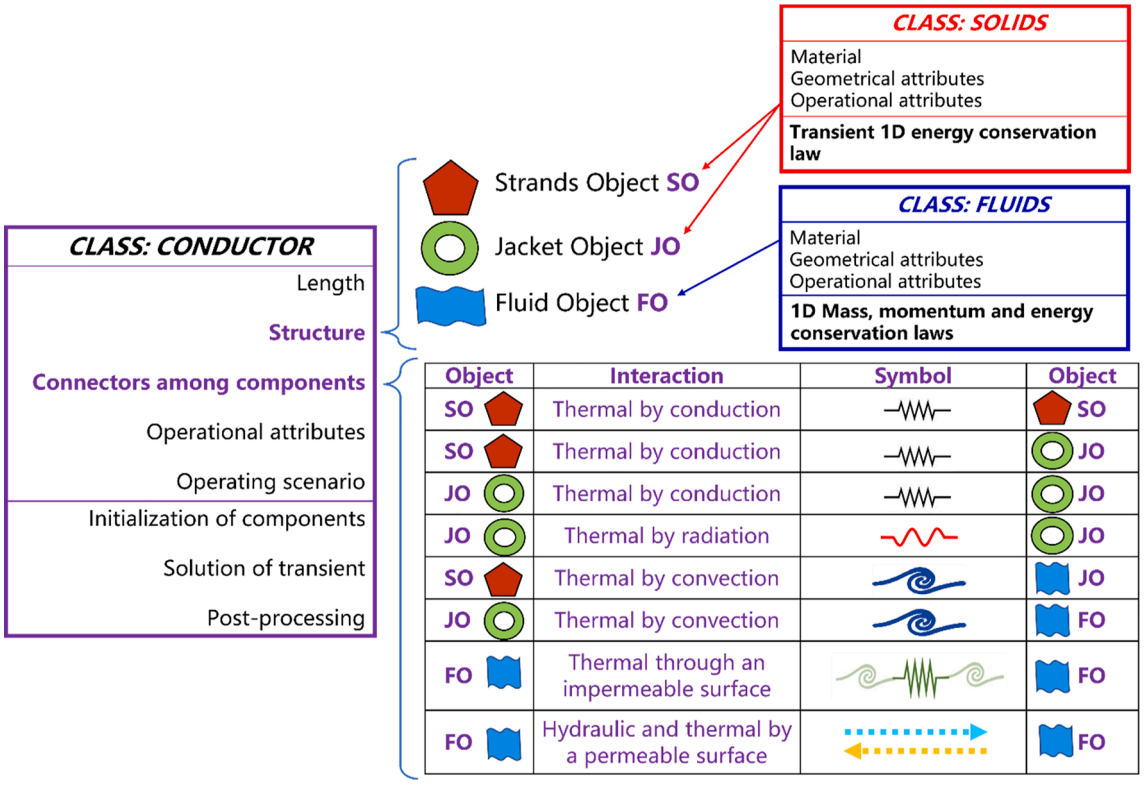

Fig. 6. Schematic view of the class of Conductors, with attributes and properties, with the nested objects from the class of Strands and Fluids, and their possible connections. The symbols to identify **SO**s, **JO**s and **FO**s are also reported, as well as the symbols for the connectors among them.

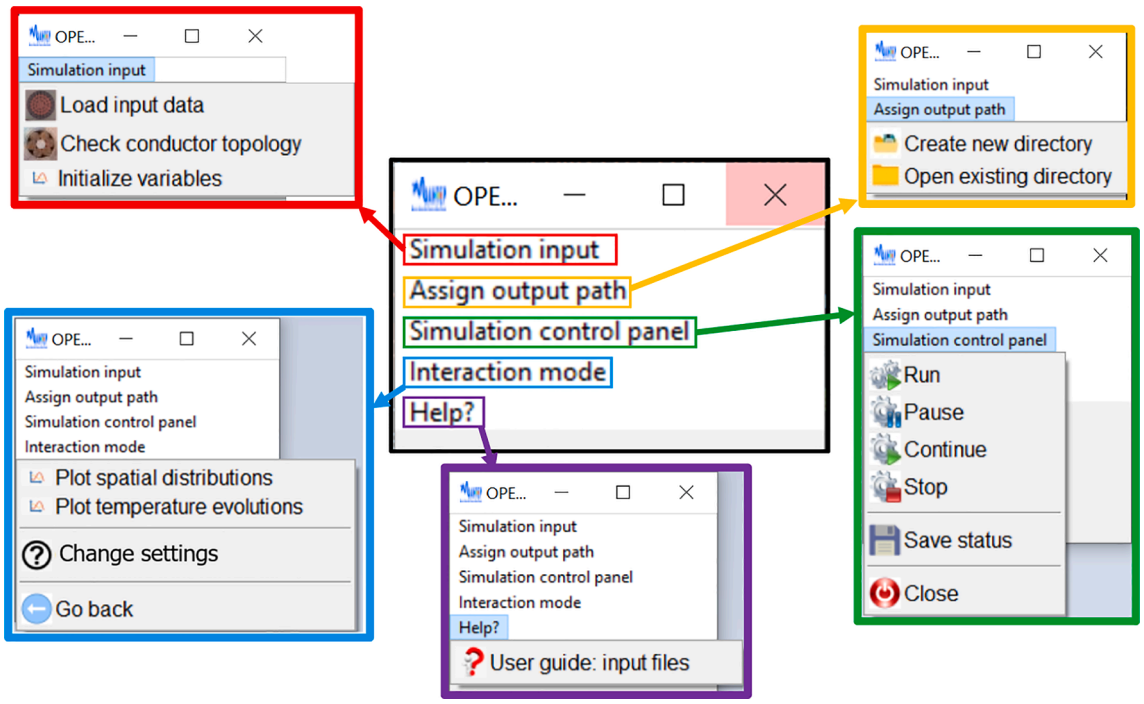

Fig. 7. Collection of the main and satellite windows of the OPENSC^2 GUI.

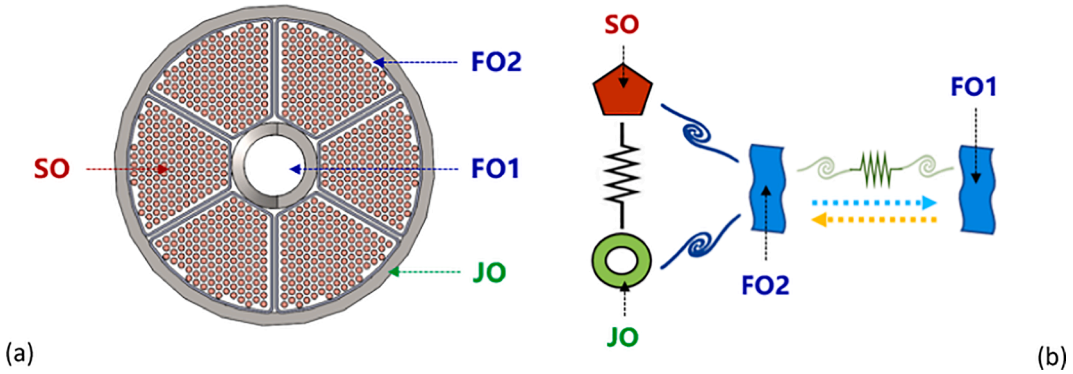

Fig. 8. (a) Sketch of the cross section of the cable adopted for the ITER Toroidal Field Coil and (b) sketch of corresponding OPENSC^2 model. FO1 is the central channel fluid, FO2 is the bundle fluid, SO represents the strand bundle and JO represents the jacket in the conductor model.

second corrugated pipe, around which the thermal and electrical insulation is wrapped. This is constituted by Polypropylene Laminated Paper (PPLP) lapped by a second cryogenic fluid, GN_2, acting as a thermal shield. Note that the direction of the GN_2 could be the same of the primary coolant or opposite to that, according to the cooling scheme of the cable. A second cryogenic envelope made by two concentric corrugated pipes, vacuum separated by a spacer, confines the GN_2 on the inner side from the environment on the outer side. With respect to the cable layouts shown in Fig. 2, we select here a case for which two different cryogen fluids are simultaneously present. The transverse dimension of the cable is of tens of centimeters, while the relevant length for such cables should reach several hundreds of kilometers (but with several cooling station along the line). Fault or transient conditions could induce heat generation in the SC wires, while Joule heating is entering the cable from the terminations. All along the cable, a parasitic load also enters the cable by either convection/radiation or conduction.

The OPENSC^2 objective for the test against a HTS power-transmission cables is to demonstrate the capability to correctly reproduce the temperature profile along a 0.1 km-long cable, the simplified geometry of which is given in Table 2, during its standard operation, accounting for radiative heating from the environment and the two cryogens in counterflow. The numerical test should fail when the behavior expected from a counter-current heat exchanger is violated, and the conservation of the energy transferred by radiation from the environment to the two cryogens fails.

The thermal–hydraulic modeling of such cable requires 1D models for the different components, suitably thermally coupled along their length. The new modeling ingredients that are necessary to exhaustively capture the thermal–hydraulic behavior of such cable, if compared to the previous test cases, include the need to model:

1) Simultaneously different cryogenic fluid within the same cable model.
2) Simultaneously different flow directions for the fluids in the same cable model.
3) The multi-wall cryostat configuration.
4) The heat transfer by radiation within different jackets to account for the cryogenic envelope.

Table 3
Test 1: geometrical and operation attributes of the selected ITER TF-like conductor.

Parameter	Unit	Value
Strand perimeter wetted by bundle channel fluid (SO-FO2 contact)	m	3.728
Strand perimeter wetted by central channel fluid (SO-FO1 contact)	m	0.0
Jacket perimeter wetted by bundle channel fluid (JO-FO2 contact)	m	0.094
Jacket perimeter wetted by central channel fluid (JO-FO1 contact)	m	0.0
Jacket – strand contact perimeter (JO-SO contact)	m	0.031
Bundle channel central channel wetted perimeter (FO1-FO2 contact)	m	0.028
h between strand and bundle channel fluid	$W/m^2/K$	1000
h between jacket and bundle channel fluid	$W/m^2/K$	1000
h between jacket and strand	$W/m^2/K$	500
h between bundle channel fluid and central channel fluid	$W/m^2/K$	1000
Friction factor bundle channel		0.02
Friction factor central channel		0.02

3. Development of a novel object-oriented tool

The OPENSC^2 tool has been developed following an object-oriented approach, using Python as the programming language. The object-oriented approach relies on the definition of objects as children of a specific component class, from which they inherit attributes (that are properties) and methods (that define what the objects should be able to do).

The constitutive class for the OPENSC^2 tool is the class of CONDUCTORS, see Fig. 6.

3.1. Attributes of objects in the conductor class

The first attribute of each object instantiated by the Conductors class (Conductor Object, **CO**), is the length of the conductor, taken along its axis, which could differ from the axis taken along the different conductor components. In fact, the strands, for instance, are twisted before their insertion in the jacket, so that their axes are typically inclined with respect to the conductor axis. The second attribute of each **CO** is the structure, defined by its basic components and their connections. The components are grasped as objects belonging in turn to two different classes: the class SOLIDS and the class FLUIDS.

Two kinds of children objects can be derived from the class SOLIDS and namely the Strand Objects (**SO**) and the Jacket Objects (**JO**). Both **SO**s and **JO**s are characterized by their materials, the properties of which are grasped from open-source material libraries, and by geometrical attributes such as the cross section and the share of different components on the cross section. The **SO**s could be modeled in fact as pure SC material, like the LTS Nb_3Sn and NbTi, or pure stabilizer (copper, aluminum, …) or as a mixture of SC materials and stabilizer, as for the HTS tapes. In the latter case, the volume ratio between the different constituting materials is specified as an attribute, and the thermophysical properties of the mixture are computed as a mass average (for the specific heat c_p) or a volume average (for the thermal conductivity k) of the properties of the original materials. Moreover, for the **JO**s different materials (either structural and insulating, see Table 1 for example) are available. For any objects, the object angle θ with respect to the cable axis should be also specified. The method the class SOLIDS prescribes to its objects is the compliance with the 1D energy conservation law, see Section 3.2.

If operation attributes can vary between the different **CO** component, it is reasonable that they can become attributes of the different components rather than of the whole **CO**. In the attributes qualifying the thermal–hydraulic drivers, the possible presence of "external" heating is included, either by specifying initial and final coordinates of the heating zone along the object, the amount of heating power per unit length (in (W/m)), and the duration of the heating, or reading suitable tables specifying the same information. The attributes qualifying the electromagnetic conditions allow specifying a value of the magnetic field for any **SO**s and **JO**s, along the respective axis, and the transport current for any **SO**s. Both aspects are relevant to properly compute the current distribution in the cable and its evolution, as reported in [60].

Children objects instantiated in the class FLUIDS are Fluid Objects (**FO**). **FO**s are characterized by a specific medium, the properties of which are grasped from CoolProp library, geometrical attributes such as the cross section and the hydraulic diameter and hydraulic attributes like the friction factor. The methods of the class FLUIDS are the 1D mass/momentum and energy conservation laws.

Among the other attributes of the **CO**s we find the connectors among the different **SO**s, **JO**s and **FO**s, that can be chosen among different possible alternatives, according to the actual topology of the conductor. Any object of the SOLIDS class can be connected to any other **SO**s and **JO**s by a conductive thermal coupling, and in that case the conductive thermal resistance per unit length R_{cond} between them, as defined in Eq (1), must be specified.

$$R_{cond} = \frac{r_{i,l}}{A'_{i,l}} \tag{1}$$

In Eq. (1), A′ in (m) is the contact area per unit length along the conductor axis (resulting in a contact perimeter), r is the contact thermal resistance in $\left(\frac{m^2K}{W}\right)$, i stays for the generic **SO** and l stays either for the generic **SO** or **JO** connected to the i-th object.

As a main difference with respect to the **SO**s, the **JO**s can be connected to other **JO**s also by radiative thermal coupling. In view of the separation of the space scales, the heat transfer by radiation is assumed to be local along the cable, i.e. each cable segment transfers heat by radiation only to the facing segment. Furthermore, each **JO** acting as an envelope for the innermost **JO**s is assumed to absorb all the reflected radiation, while for all the innermost **JO**s, assumed to be at a comparable temperature (no mutual connection by radiative heat transfer), the effect of reflectance radiosity is accounted for. For all **JO**s, the grey-body approximation is retained (the emissivity is assumed to be constant). Under the above assumptions, the thermal resistance per unit length R_{rad} comes from the linearization of the heat transfer by radiation and is defined in Eq. (2) for the **JO**s encompassed within a **JO** acting as an envelope:

$$R_{rad} = \frac{\frac{1-\varepsilon_i}{A'_i\varepsilon_i} + \frac{1}{A'_i F_{i,j_{env}}}}{\sigma\left(T_{j_{env}}^2 + T_i^2\right) \times \left(T_{j_{env}} + T_i\right)} \tag{2}$$

In Eq. (2), i stays for the **JO** object under consideration, A' in (m) is the radiating area per unit length along the conductor axis, $F_{i,j_{env}}$ is the view factor between the **JO** object under consideration and the one acting as envelope, ε_i is the surface emissivity of the **JO** object, σ is the Stefan-Boltzmann constant, $T_{j_{env}}$ and T_i are the temperature of the **JO** object acting as envelope and of the **JO** object under consideration, respectively.

Any object of the SOLIDS class can be connected to one or more **FO**s by a convective thermal coupling, and in that case the convective thermal resistance per unit length R_{conv} between them, as defined in Eq. (3), must be specified.

$$R_{conv} = \frac{1}{A'_{i,f} h_{i,f}} \tag{3}$$

In Eq. (3), A′ in (m) is the contact area per unit length along the conductor axis, h is the heat transfer coefficient in $\left(\frac{W}{m^2K}\right)$, i stays for the generic **SO** or **FO** and f stays for the generic **FO** connected to the i-th

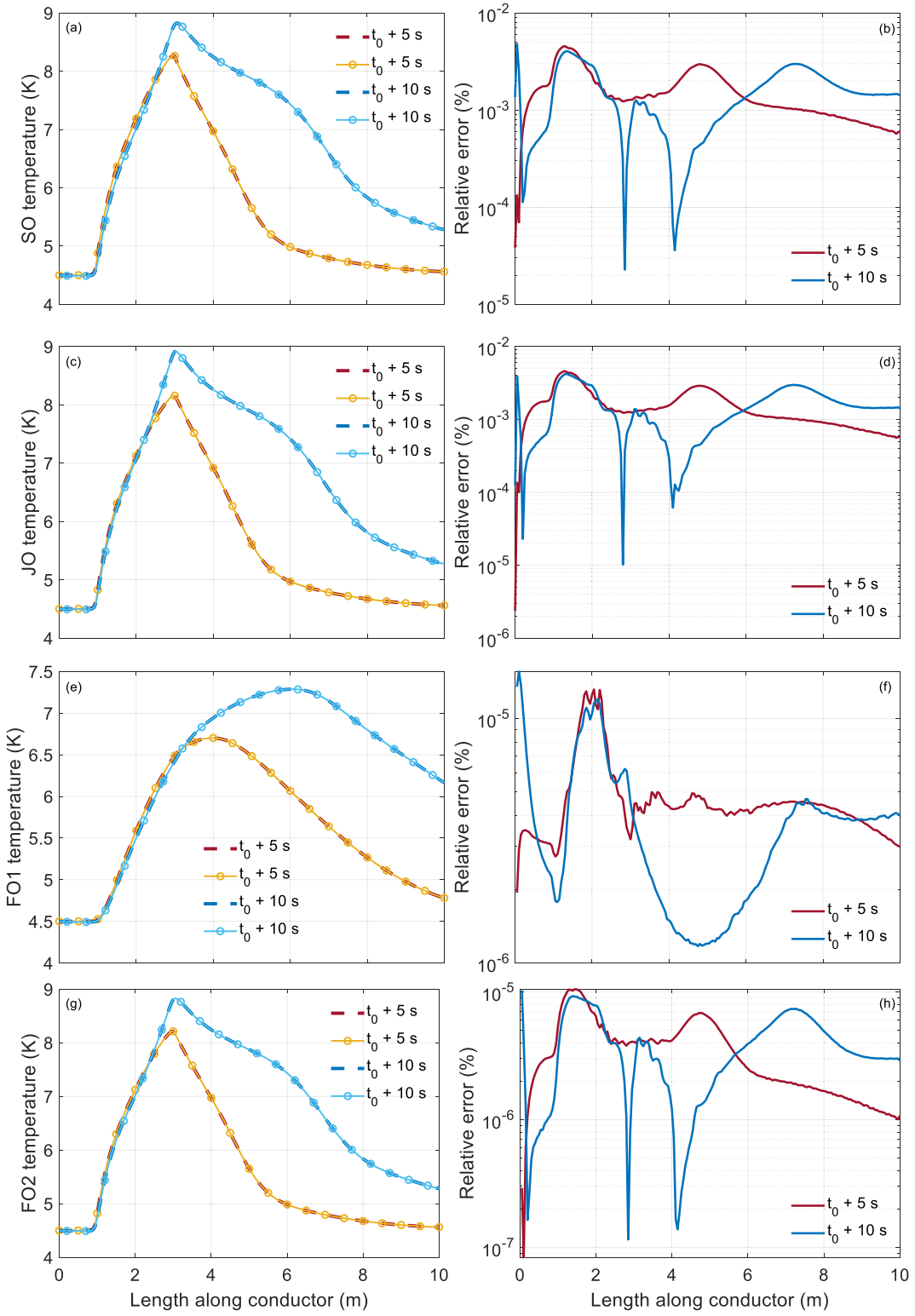

Fig. 9. Test 1: spatial temperature profiles computed with OPENSC^2 (dashed lines) and 4C (solid-marked lines) at 5 s and 10 s after the beginning of the heating at t_0, in the case of given v_{in}, T_{in} and p_{out} for the FOs: (a) SO temperature and (b) corresponding relative error; (c) JO temperature and (d) corresponding relative error; (e) FO1 temperature vs the "hole" temperature from 4C and (f) corresponding relative error; (g) FO2 temperature vs the "bundle" temperature from 4C and (h) corresponding relative error.

object.

The last connectors, i.e. those between different **FO**s, need for their definition the additional attribute of the open surface fraction between the objects: an open fraction equal to one would describe a fully permeable interface between two **FO**s, while an open fraction equal to zero would describe a fully impermeable interface between two **FO**s. In the latter case, the two **FO**s are interconnected by the heat transfer through the impermeable surface in between. In that case the thermal resistance per unit length R_{mix} between them, defined as a series of (convective and conductive) thermal resistances in Eq (4), needs to be

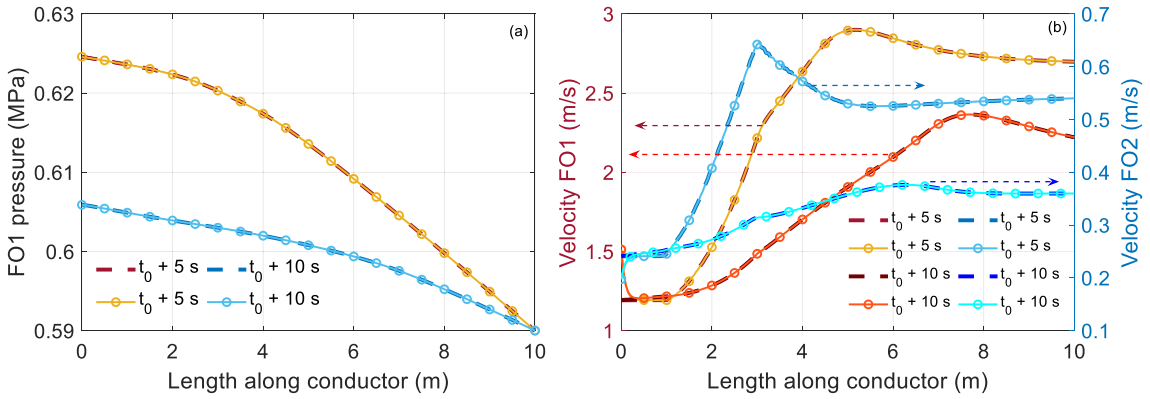

Fig. 10. Test 1: spatial profiles of hydraulic variables computed with OPENSC^2 (dashed lines) and 4C (solid-marked lines) at 5 s and 10 s after the beginning of the heating at t_0 in the case of given v_{in}, T_{in} and p_{out} for the FOs: (a) FO1 pressure vs the "hole" pressure from 4C and (b) (left axis) FO1 velocity vs the "hole" velocity from 4C and (right axis) FO2 velocity vs the "bundle" velocity from 4C.

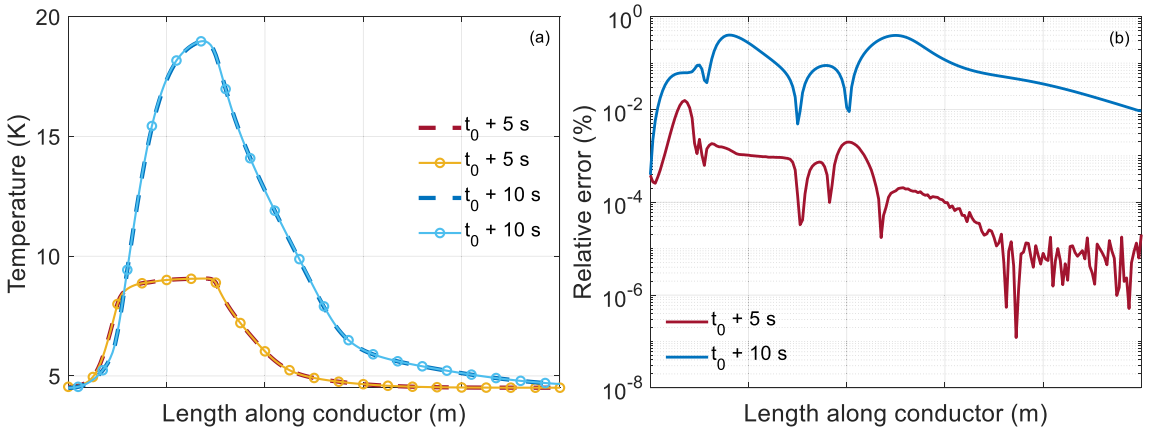

Fig. 11. Test 1. Test 1: spatial temperature profiles computed with OPENSC^2 (dashed lines) and 4C (solid-marked lines) at 5 s and 10 s after the beginning of the heating at t_0, in the case of given p_{in}, T_{in} and p_{out} for the FOs: (a) SO temperature, with (b) corresponding relative error.

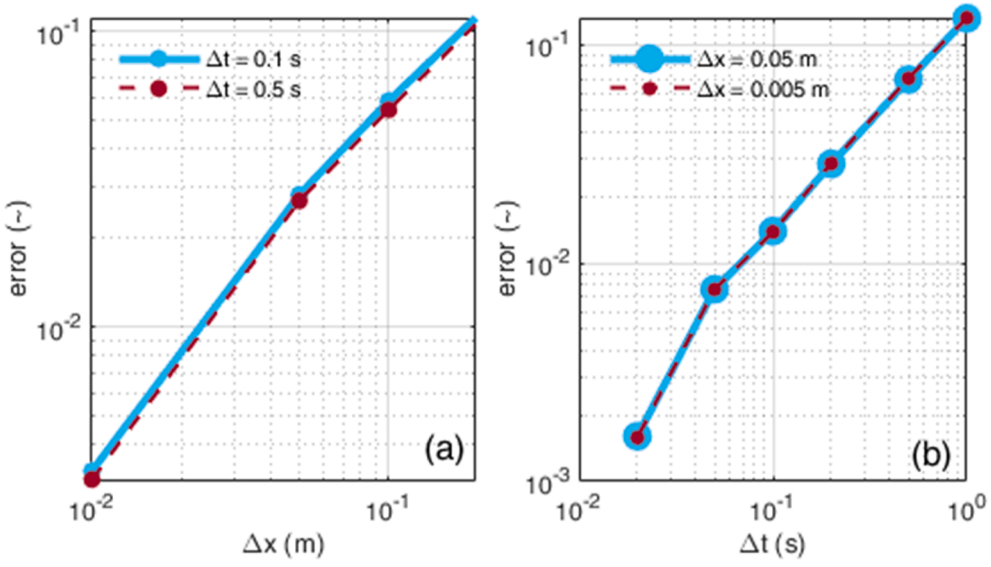

Fig. 12. Space (a) and time (b) convergence plots for the Test 1 simulation.

specified:

$$R_{mix} = \frac{1}{h_i} + \frac{z}{k} + \frac{1}{h_l} \tag{4}$$

In Eq. (4), i and l stay for the generic **FO** objects in contact, h is the heat transfer coefficient in $\left(\frac{\mathrm{W}}{\mathrm{m^2K}}\right)$, k and z are the thermal conductivity in $\left(\frac{\mathrm{W}}{\mathrm{mK}}\right)$ and thickness in (m) of the impermeable interface between the **FO**s,

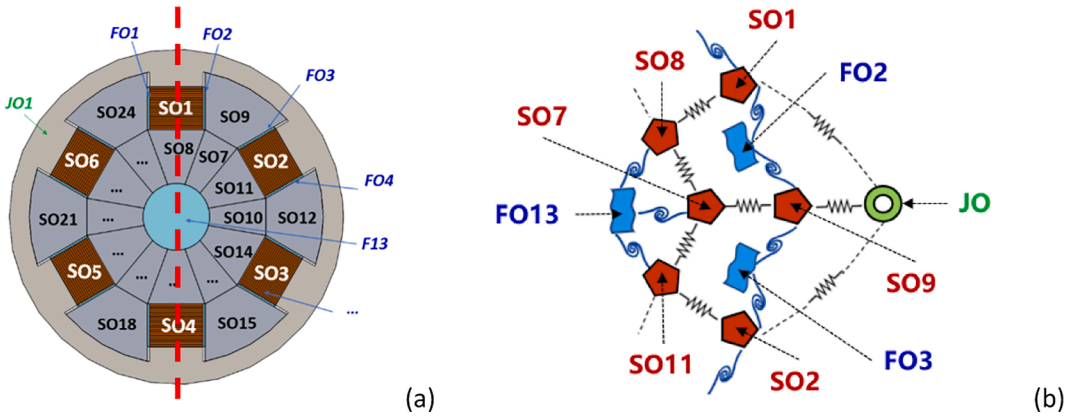

Fig. 13. Sketch of a slotted-core HTS cable for fusion applications, with the SOs and FOs numbered. SO1-SO6 correspond to the HTS tapes stacks, all the other SOs discretize on the cross section the slotted core of the conductor. JO1 is the jacket. FO1-FO12 model the side channels in the slots where the tapes are inserted, while FO13 is the central channel. (b) OPENSC^2 sketch of a portion corresponding to 1/6 of the cable cross section.

respectively, under the assumption that it is thin, so that the approximation to the flat slab for the thermal resistance holds. In case the connection between two **FO**s occurs through a permeable surface it is much more complex, since the transfer of momentum and energy are driven by the transfer of mass between the two objects, see [61] for more details. While in principle the coupling among the different objects could vary along their length, for the time being it is assumed that all the couplings remain the same throughout the entire length of the **CO**. Under this assumption, the effect of the contact resistance between different objects can be easily assessed by means of dedicated parametric analyses, testing the data taken for any specific parameter of interest in a suitably wide range.

The operational attributes for the **CO** are the type of transient and duration of the transient that is under investigation, as well as the operating scenario of the conductor. The Type of transient (Pure-hydraulic, DC-performance, AC-performance, Quench, …) and operating scenario allow switching on/off specific features of the model. If the operation concerns specifically current scenarios, it is discussed in detail in [60] and are outside the scope of this paper, the focus of which is on the thermal-fluid dynamic model of the SC cables. The duration of the transient allows setting the end time of the simulation, performed according to the methods defined for the **CO**.

The object-oriented approach to the construction of the OPENSC^2 code ensures that several **CO**s can be defined in the same model and simulated within the same simulation framework. Currently, multi-conductor simulations with no interactions between the **CO**s are possible, as done in [62], where the different **CO**s can also benefit of different durations of their transients. Note, however, that the interaction of different **CO**s will call for a higher-level class of objects, say the WINDING PACK class, to be addressed in the future.

3.2. Methods of objects in the conductor class

The methods defined for each instance of the conductor class include the initialization of the components at their operating conditions and the solution of the transient, defined by the operating scenario, together with the post-processing of the results, see Fig. 6.

The specific method adopted in OPENSC^2 for the solution of the transient for the **SO**s and **JO**s, when they become a part of a **CO**, assumes that they are characterized by a single thermal–hydraulic variable, the temperature T, that needs to be assessed during any transient evolution of the **CO** through the 1D transient heat conduction equation. The model for the **SO**s and **JO**s includes then a first part inherited from the class SOLIDS, that is the basic 1D transient energy conservation law, i.e. the left-hand side of Eq. (5) and Eq. (6) for any **SO**s and any **JO**s, respectively. At the right-hand side of Eq. (5), the source term per unit length $Q_{operation}(t,x)$, (in (W/m)), is defined by the operating conditions and scenario, while the other terms refer to all the possible connectors to the other objects, components of the same **CO**, as summarized in Fig. 6. In Eq. (6) the peculiar contribution of power entering the jacket from the environment per unit length is also present, which refers to the coupling to the class of objects ENVIRONMENT, characterized by the "environmental temperature" as its attribute, together with the presence of a fluid (air) and respective temperature.

$$A_i\rho_i c_{p,i}\frac{\partial T_i}{\partial t}-A_i\frac{\partial}{\partial x}\left(k_i\frac{\partial T_i}{\partial x}\right)=Q_{operation}(t,x)+\sum_{s\neq i}^{N_S}\frac{(T_s-T_i)}{R_{cond,i,s}}+\sum_{j=1}^{N_J}\frac{(T_j-T_i)}{R_{cond,i,j}}+\sum_{f=1}^{N_F}\frac{(T_f-T_i)}{R_{conv,i,f}} \tag{5}$$

$$A_i\rho_i c_{p,i}\frac{\partial T_i}{\partial t}-A_i\frac{\partial}{\partial x}\left(k_i\frac{\partial T_i}{\partial x}\right)=Q_{environment}(t,x)+Q_{operation}(t,x)+\sum_{s=1}^{N_S}\frac{(T_s-T_i)}{R_{cond,i,s}}+\sum_{j\neq i}^{N_J}\frac{(T_j-T_i)}{R_{cond,i,j}}+\sum_{j\neq i}^{N_J}\frac{(T_j-T_i)}{R_{rad,i,j}}+\sum_{f=1}^{N_F}\frac{(T_f-T_i)}{R_{conv,i,f}} \tag{6}$$

In Eq. (5), i refers to the **SO** under consideration, s refers to the generic **SO** connected to the i-th **SO**, j is the generic **JO** connected to the i-th **SO**, f is the generic **FO** connected to the i-th **SO**. The variables t and x are the independent variable time and curvilinear spatial coordinate along the conductor axis, and ρ is the density of the media attributed to the i-th **SO**. Note that, in the case the axis of the **SO** under consideration is not parallel to that of the **CO**, $A_i = A_{\perp,i}/\cos(\theta)$, being $A_{\perp,i}$ the perpendicular cross section, and θ the angle between the **CO** axis and the **SO** axis. Finally N_F, N_J and N_S are respectively the total number of initialized **FO**s, **JO**s and **SO**s. Similarly, in Eq (6), i is the **JO** under consideration, s is the generic **SO** connected to the i-th **JO**, j is the generic **JO** connected by thermal conduction or by radiative heat transfer to the i-th **JO**, f is the generic **FO** connected to the i-th **JO**. For **SO**s and **JO**s, adiabatic conditions are always prescribed at both boundaries, as done for instance in [61,63].

As a main difference with respect to the **SO**s and **JO**s, the method for each **FO** accounted for in the **CO** structure includes equations not only for its average temperature on the cross section, but also for its average velocity v and pressure p. A set of 1D equations describing the conservation of mass and momentum for a compressible inviscid single-phase fluid (Euler equations) is written together with an equation describing the thermal energy conservation. This form has been selected for the conservation laws since it allows an accurate description of the transient behavior for gasses in cryogenic conditions, for which viscous

Table 4
Test 2: Geometrical attributes of the selected slotted-core HTS cable for fusion.

Parameter	Unit	Value/Correlation
Cross section for SO1-6 (type1 SO)	mm^2	12.8
Material of SO1-6		HTS
Cross section for SO9, 12, 15, 18, 21, 24 (type2 SO)	mm^2	21.06
Material of SO9, 12, 15, 18, 21, 24		Aluminium
Cross section for SO8, 11, 14, 17, 20, 23 (type3 SO)	mm^2	11.32
Material of SO8, 11, 14, 17, 20, 23		Aluminium
Cross section for SO7, 10, 13, 16, 19, 22 (type4 SO)	mm^2	8.61
Material of SO7, 10, 13, 16, 19, 22		Aluminium
Contact perimeter between SOs (type1 to type3)	mm	4.00
r between SOs (type1 to type3)	m^2K/W	$3x10^{-5}$
Contact perimeter between SOs (type3 to type4)	mm	4.34
r between SOs (type3 to type4)	m^2K/W	$5x10^{-6}$
Contact perimeter between SOs (type2 to type4)	mm	2.76
r between SOs (type2 to type4)	m^2K/W	$5x10^{-6}$
Cross section for JO	mm^2	139.7
Material of JO		Stainless steel
Contact perimeter between type1 SOs and jacket	mm	4.0
r between type1 SOs and jacket	m^2K/W	∞
Contact perimeter between type2 SOs and jacket	mm	7.19
r between type2 SOs and jacket	m^2K/W	$8.8x10^{-4}$
Cross section of FO1-12 (type1 FO)	mm^2	0.65
Material of FO1-12		SHe
Cross section of FO13 (type2 FO)	mm^2	19.64
Material of FO13		SHe
Contact perimeter between type1 FOs and type1 SOs	mm	3.23
h between type1 FOs and type1 SOs	$W/m^2/K$	Dittus-Boelter correlation: $h = k/D_h 0.023 Re^{0.8} Pr^{0.3}$
Contact perimeter between type1 FOs and type2 SOs	mm	4.3
h between type1 FOs and type2 SOs	$W/m^2/K$	Dittus-Boelter correlation: $h = k/D_h 0.023 Re^{0.8} Pr^{0.3}$
Contact perimeter between type1 FOs and type3 SOs	mm	0.15
h between type1 FOs and type3 SOs	$W/m^2/K$	Dittus-Boelter correlation: $h = k/D_h 0.023 Re^{0.8} Pr^{0.3}$
Contact perimeter between type1 FOs and type4 SOs	mm	0.0
h between type1 FOs and type4 SOs	$W/m^2/K$	0.0
Contact perimeter between type-1 FOs and jacket	mm	1.25
h between type1 FOs and JO	$W/m^2/K$	0.0
Contact perimeter between type-2 FO and type-3 SOs	mm	1.31
h between type-2 FO and type-3 SOs	$W/m^2/K$	Dittus-Boelter correlation: $h = k/D_h 0.023 Re^{0.8} Pr^{0.3}$
Contact perimeter between type-2 FO and type-4 SOs	mm	1.31
h between type2 FO and type4 SOs	$W/m^2/K$	Dittus-Boelter correlation: $h = k/D_h 0.023 Re^{0.8} Pr^{0.3}$
Friction factor for type1 FOs		$f = \begin{cases} 0.316 Re^{-0.25}, Re \leq 1e4 \\ 2.21 Re^{-}0.4, Re > 1e4 \end{cases}$
Friction factor for type2 FO		$\frac{1}{\sqrt{f}} = -2\log_{10}\left(\frac{\varepsilon}{3.7D_h} + \frac{2.51}{Re\sqrt{f}}\right)$

dissipative effects are small, capturing at the same time the effects of pressure. This method is particularly suitable for SHe and GN_2. In the future, methods for uncompressible cryogens with a simplified modeling of the two-phase transition could be implemented to account for the LN_2.

The original conservation laws are customarily manipulated to obtain a set of equivalent equations in the non-conservative variables v, p, T, substituting the original variable ρ, v, u, where u is the specific internal energy of the fluid, as reported in Eq. (7). This approach has been successfully applied both in Gandalf / THEA / SUPERMAGNET [63,64] and in Mithrandir / 4C [48,65], while in VINCENTA / VENICIA the fluid enthalpy w [66] is preferred with respect to the temperature.

$$\begin{cases} \dfrac{\partial v_i}{\partial t} + v_i\dfrac{\partial v_i}{\partial x} + \dfrac{1}{\rho_i}\dfrac{\partial p_i}{\partial x} = \dfrac{1}{\rho_i}\ \Lambda_{v+\rho} \\ \dfrac{\partial p_i}{\partial t} + \rho_i c_s^2\dfrac{\partial v_i}{\partial x} + v_i\dfrac{\partial p_i}{\partial x} = \dfrac{\Phi_i}{A_i}\left[F + \sum_{s=1}^{N_S}\dfrac{(T_s - T_i)}{R_{cond,i,s}} + \sum_{j=1}^{N_J}\dfrac{(T_j - T_i)}{R_{cond,i,j}} + \sum_{f\neq i}^{N_F}\dfrac{(T_f - T_i)}{R_{mix,i,f}} + \sum_{f\neq i}^{N_F}\Lambda_{\rho+v+e,i}\right] \\ \dfrac{\partial T_i}{\partial t} + \Phi_i T_i\dfrac{\partial v_i}{\partial x} + v_i\dfrac{\partial T_i}{\partial x} = \dfrac{1}{A_i\rho_i c_{v,i}}\left[F + \sum_{s=1}^{N_S}\dfrac{(T_s - T_i)}{R_{cond,i,s}} + \sum_{j=1}^{N_J}\dfrac{(T_j - T_i)}{R_{cond,i,j}} + \sum_{f\neq i}^{N_F}\dfrac{(T_f - T_i)}{R_{mix,i,f}} + \sum_{f\neq i}^{N_F}\Lambda_{\rho' +v+e,i}\right] \end{cases} \quad (7)$$

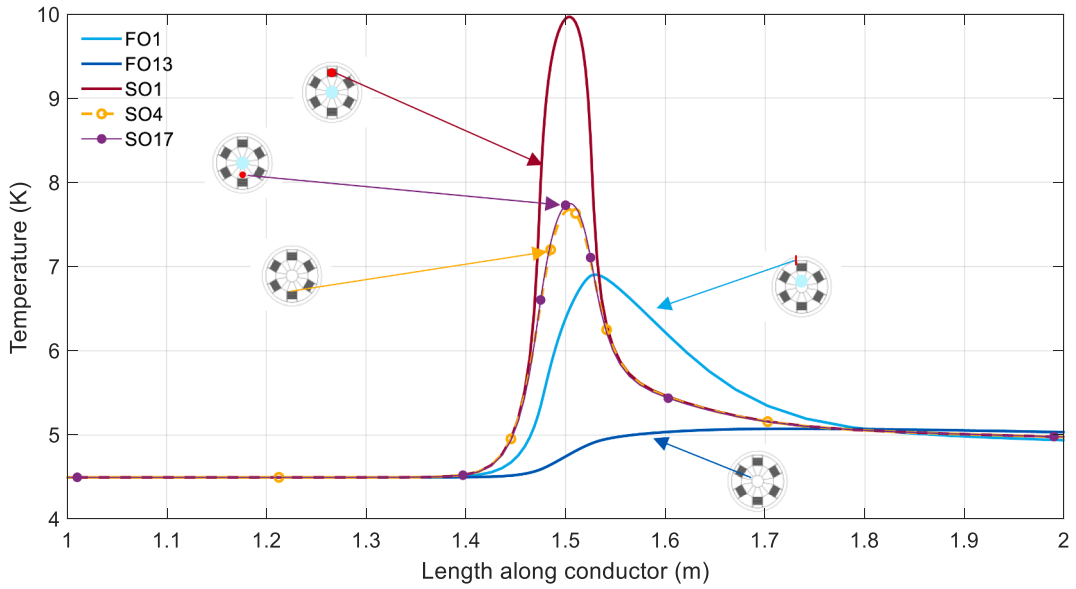

Fig. 14. Test 2: computed temperature profiles of different **SO**s on the red line in Fig. 13a, at the end of the heating of **SO1**. The profiles computed for **FO1** and **FO13** are also reported.

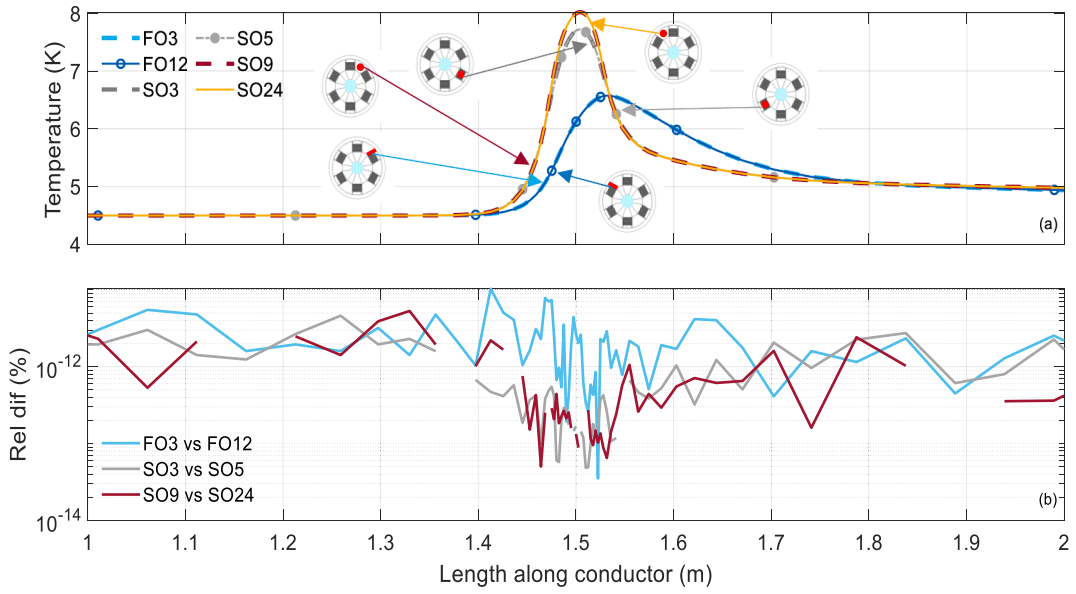

Fig. 15. Test 2: (a) Computed temperature profiles of **FO**s and **SO**s located symmetrically to **SO1** at the end of the heating. (b) Relative difference for the couples of symmetrical objects.

In the set of Eq. (7), i is the **FO** under consideration, s is the generic **SO** connected to the i-th **FO**, j is the generic **JO** connected to the i-th **FO**, f is the generic **FO** connected to the i-th **FO** through an impermeable surface. Looking at the coefficients, c_s is the sound speed, c_v is the specific heat at constant volume, Φ is the Gruneisen parameter and F is the friction term defined in Eq. (8).

$$F = \frac{2 f_{fric} v_i^2}{D_{h,i}} \rho_i v_i A_i \tag{8}$$

where f_{fric} is the friction factor and $D_{h,i}$ is the hydraulic diameter of the i-th **FO**.

The connection to another **FO** through a permeable surface occurs through the source terms $\Lambda_{v+\rho}, \Lambda_{\rho+v+e}, \Lambda_{\rho'+v+e}$, respectively, driven by the unbalance of pressure between the two connected **FO**s. If the pressure unbalance $\left(p_f - p_i\right) \rangle 0$, the i-th **FO** receives mass, momentum and energy from the connected **FO** f, while if the pressure unbalance $\left(p_f - p_i\right) \langle 0$, the i-th **FO** feeds the connected **FO** f with mass, energy and momentum. The coupling terms among connected **FO**s are crucial to correctly reproduce the thermal–hydraulic transients in ITER-like conductors for fusion, but the actual permeable surface available for the mass / momentum / energy transfer between neighboring hydraulic channels is very difficult to assess (also due to the presence of wrapping around the strands, that can chock the flow among the channels), and needs to be calibrated. As a final remark on the set of the equations for the **FO**s, the method described by Eq. (7) is highly non-linear, since all the coefficients representing thermophysical properties of the fluid are functions of both pressure and temperature. A suitable numeric treatment for such strong non-linearity deserves some attention, see below.

For the **FO**s the boundary conditions, in the form of operation attributes, are specified according to the characteristic theory. For the

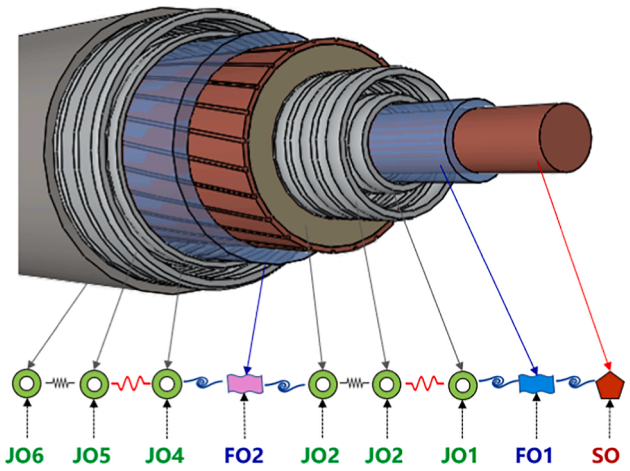

Fig. 16. Sketch of the 4-wall cryostat HTS SC cable adopted in Test 3 (top) and the corresponding OPENSC^2 model (bottom). FO1 models the inner coolant, FO2 the outer coolant, JO1 the inner cryostat (inner wall), JO2 the inner cryostat (outer wall), JO3 the insulator & electric shield; JO4 the outer cryostat (inner wall), JO5 the outer cryostat (outer wall), JO6 the outer insulation and finally SO the SC wires + stabilizer.

Table 5
Test 3: Operational attributes of the HTS SC cable for power transmission.

Parameter	Unit	Value/correlation
Contact perimeter between environment and JO6	m	0.584
Contact perimeter between FO1 and SO1	m	0.031
Contact perimeter between FO1 and JO1	m	0.063
Contact perimeter between FO2 and JO3	m	0.339
Contact perimeter between FO2 and JO4	m	0.402
Contact perimeter between JO1 and JO2	m	0.075
Contact perimeter between JO2 and JO3	m	0.151
Contact perimeter between JO4 and JO5	m	0.415
Contact perimeter between JO5 and JO6	m	0.490
h between environment and JO6	W/ m^2/K	5
h between FO1 and SO1	W/ m^2/K	Dittus-Boelter correlation:$h = k/D_h 0.023 Re^{0.8} Pr^{0.3}$
h between FO1 and JO1	W/ m^2/K	Dittus-Boelter correlation:$h = k/D_h 0.023 Re^{0.8} Pr^{0.3}$
h between FO2 and JO3	W/ m^2/K	Dittus-Boelter correlation:$h = k/D_h 0.023 Re^{0.8} Pr^{0.3}$
h between FO2 and JO4	W/ m^2/K	Dittus-Boelter correlation:$h = k/D_h 0.023 Re^{0.8} Pr^{0.3}$
h between JO1 and JO2	W/ m^2/K	From Eq. (2)
h between JO2 and JO3	W/ m^2/K	500
h between JO4 and JO5	W/ m^2/K	From Eq. (2)
h between JO5 and JO6	W/ m^2/K	500
Friction factor FO1		0.02
Friction factor FO2		0.02

conservation laws written in the non-conservative variables p and T, a subsonic flow from an upstream volume (manifold) at given pressure and temperature to a downstream volume (manifold) at given pressure and temperature corresponds to two entering characteristics and one exiting characteristic. Two variables must be then specified at the **FO** inlet, and one at its outlet. Several alternatives are available in OPENSC^2, among which:

Impose the inlet pressure p_{in} and temperature T_{in} and the outlet pressure p_{out}
Impose the inlet v_{in} and T_{in}, together with p_{out}

Any of the above-listed choices can be attributed to a **FO** as a value constant in time, or prescribing its time evolution in suitable tabular form.

3.3. Numerics

Once the **CO** is built from the basic **SO**s, **JO**s and **FO**s, and the methods (equations) associated to each of them and their connections have been clarified, a suitable numerical solution scheme for the resulting set of equations should be identified. In view of the presence of several coupling terms between the constitutive equations for the different objects, and, in the perspective of keeping the code flexibility as high as possible, the possibility to simulate transients for which the time-scale for the coupling between the equations is faster or comparable to that of the transient driver should be addressed. That calls for an implicit scheme for the coupling of the parabolic-hyperbolic system of Partial Differential Equations (PDEs) describing the different cable elements. A vector of the solution unknowns $\boldsymbol{U}(t,x)$, function of the variables time t and curvilinear coordinate along the conductor axis x, is built following the order used in the multi-solid multi-channels Mithrandir M^3 [67] as shown in Eq. (12).

$$\boldsymbol{U}(t,x) = \left[\cdots \quad v_{fi} \quad p_{fi}\ T_{fi} \quad \cdots \quad T_{si} \cdots \quad T_{ji} \right]^T \tag{12}$$

where the index *fi* refers to the generic **FO**, *si* refers to the generic **SO** and *ji* refers to the generic **JO**. The size M of the vector $\boldsymbol{U}$ then equals $M = 3N_F + N_S + N_J$.

The problem can be then written in matrix from as in Eq. (13):

$$\mathbb{M}\frac{\partial \boldsymbol{U}}{\partial t} + \mathbb{A}\frac{\partial \boldsymbol{U}}{\partial x} - \frac{\partial}{\partial x}\left(\mathbb{K}\frac{\partial \boldsymbol{U}}{\partial x}\right) + \mathbb{S}\boldsymbol{U} = \mathbb{Q} \tag{13}$$

where the matrix $\mathbb{S}$ contains the coupling terms and $\mathbb{Q}$ the external sources as defined by the operation attributes. For the time being, the solution of the of PDEs in Eq. (13) is performed using a finite element (FE) method in space, with local formulation and linear trial functions and coefficients evaluated at the Gauss point (note that in this regards the latter choice differs from what is done for instance in the M3 code [67], but it is preferable in view of the large non-linearity of some of the PDE coefficients). The spatial grid is static for the time being, but can be either uniform or refined in selected regions – since the electrical model has not been implemented yet, adaptive strategies, specifically useful in the case of a quench simulation, have been not implemented yet as well. A simple 1-step implicit (Euler) or semi-implicit (Crank-Nicolson) scheme is adopted for the discretization in time, with linearization of the non-linear terms performed simply by the frozen-coefficients technique. These simple recipes are also currently implemented in [48] and, at least for the spatial discretization scheme, also in [63]. They are well established in the field and have already proven to be accurate enough for the simulations of conductors for fusion applications. The linear system resulting from the space and time discretization has a coefficient matrix of size $M \times N$, where N is the number of nodes in the spatial discretization, with a band structure of width $4 \times M - 1$. The linear system is solved with a direct method by back substitution of the banded matrix.

3.4. GUI

The GUI has been developed using Tkinter package from the

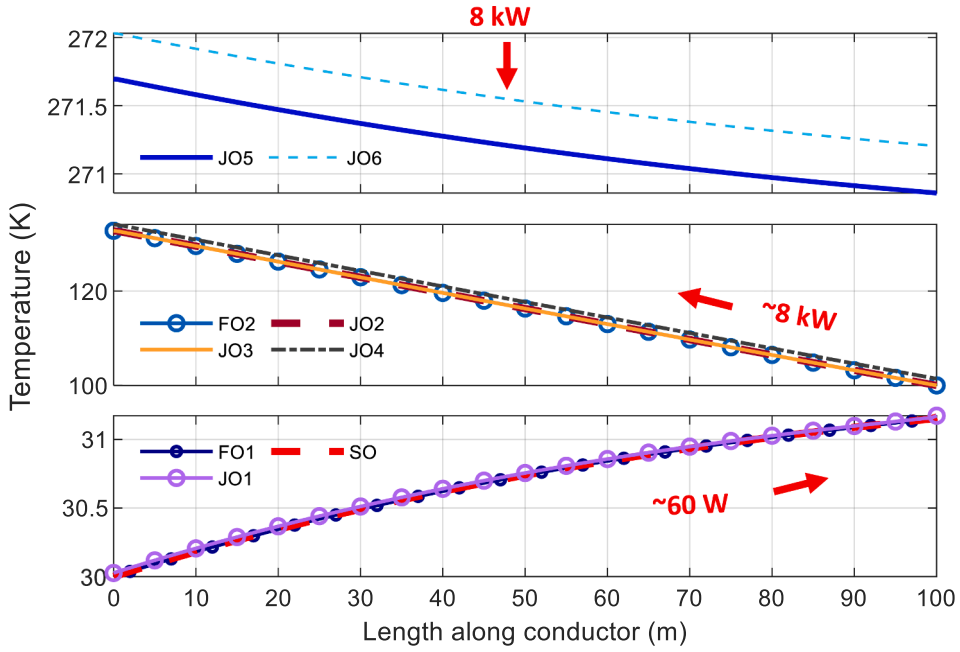

Fig. 17. Test 3: computed temperature profiles at steady state along the different **CO** components.

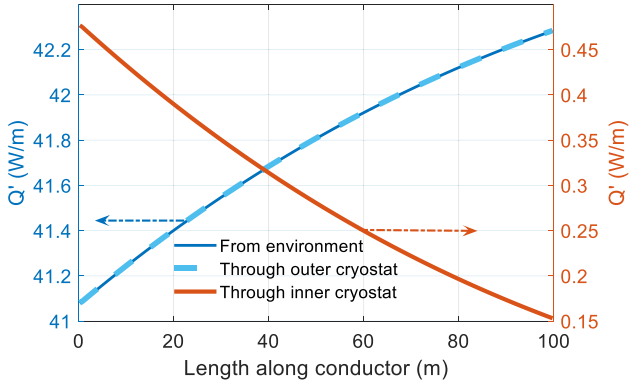

Fig. 18. Linear power density distribution: (left axis) Power per unit length transferred from the environment and outer insulation by convection, and through the shells of the outer cryostat by radiation; (right axis) Power per unit length transferred through the shells of the inner cryostat by radiation.

standard Python library, and its main features are summarized in Fig. 7. The main menu popping up as the software starts the execution allows setting the simulation input by loading the set of excel files that are used to assign the different attributes of the **CO** and its **SO**s, **JO**s and **FO**s and their connectors. Consistency of the input files can be checked by "Check conductor topology" command. Excel files are also used to assign suitable times and locations of the diagnostics, to check and plot the solution of the problem. The path for the output files can be intuitively assigned following the suggestions of the menu in "Assign output path". The simulation control panel allows running, pausing, restarting and spotting the simulations, while the "Interaction mode" allows plotting spatial distribution of the solution, as well as evolution in time of selected variables at selected locations. A user guide is available upon selection of the "Help?" entry in the menu.

4. Model validation

The model validation is presented here following the three tests identified and described in Section 2.

4.1. Test 1

The cross section of ITER-like LTS-cable for fusion (see figure Fig. 8a) identified as the first test in the TDD allows to assemble the corresponding **CO** using 1 **SO**, 1 **JO** and 2 **FO**s, as shown in Fig. 8b. The **SO** and **JO** are thermally connected by a conductive thermal coupling, and both are connected to one of the **FO**s by a convective thermal coupling. The two **FO**s are connected by a conductive thermal coupling through an impermeable interface and by mass / momentum and energy transfer through a permeable interface. The main features of the connectors among the **CO** components, used in input also to the 4C code, are listed in Table 3, together with the numerical parameters selected for the simulations.

The computed results, for the operating conditions relying on given inlet mass flow rate, T_{in} and p_{out}, are reported in Fig. 9 for the spatial distribution of the **SO** (Fig. 9a), **JO** (Fig. 9c) and **FO**s (Fig. 9e and Fig. 9g), together with the corresponding results computed by the 4C code, showing no appreciable differences in any of the **CO** constituents at any time during the transient.

The relative errors of the OPENSC^2 solution, with respect to the 4C one, is reported in Fig. 9b, d, f, h for the different variables, respectively, showing a maximum relative difference below 0.01 %. This difference, which is higher that the machine precision, is due to the different recipe adopted by the OPENSC^2 code in the evaluation of the PDE coefficients (evaluated at the Gauss point in each cable element, versus the average of the nodal values adopted in 4C). The time evolution of the pressure and velocity in the two **FO**s, at the location corresponding to the center of the conductor, is reported in Fig. 10a and Fig. 10b, respectively, together with the corresponding evolution computed using 4C. Note that, while the optical agreement is very good for the pressure distribution in the conductor hole, the spatial distribution of the computed velocity show a visible difference at the conductor inlet. This is due to the different recipe adopted by the two software to evaluate the flow distribution in the two fluid regions – that adopted by 4C is an approximated one, which in fact forces the flow to redistribute among the two regions from the inlet guessed value according to their actual hydraulic impedance. Despite that, the average error throughout the transient remains for all the hydraulic variables below 3%.

Also in the case of given p_{in}, T_{in} and p_{out} the OPENSC^2 simulation

returns qualitatively and quantitatively the same level of agreement with the 4C results, as summarized in Fig. 11.

Detailed solution verification

As a side remark, beside the successful benchmark against the 4C code, in the case of the computed solutions performed to comply with Test 1, a detailed time and space convergence analysis has been performed on the case of given p_{in}, T_{in} and p_{out}. The outcome of the analysis is reported in Fig. 12 in terms of an average relative error with respect to the most accurate solution, among the unknowns of the entire solution. For the space convergence analysis (Fig. 12a), the study performed with two different constant time stepping returns a convergence order larger than 1, as expected from a scheme that blends a 2nd order accuracy in the **SO** and **JO** equations and a 1st order accuracy in the **FO** equations. The time convergence analysis, performed for two different values of the space element size, returns a 1st order convergence, as expected from the Backward Euler scheme adopted for the time marching, see Fig. 12b.

4.2. Test 2

Following the analysis already performed in [57], the cross section of the configuration sketched in Fig. 5 allows the assembly of the corresponding **CO** using 24 **SOs**, 1 **JO** and 13 **FOs**, as shown in Fig. 13. The geometrical attributes of the **SOs**, **JO** and **FOs** are collected in Table 4, together with the connectors among the different **CO** components. The six different **SOs** are directly connected to the two thin coolant channels (**FO1-FO12** in Fig. 13), and they are directly in (conductive) contact to both the **SOs** modeling the bottom of the stabilizer core, under the slots (**SO7, SO8, SO19, SO11, …** in Fig. 13). The latter are connected through a conductive resistance to the **SOs** separating the HTS tapes (**SO9, SO12, …** in Fig. 13). The central channel for the coolant (**FO13**) is connected by a convective resistance to the **SOs** modeling the inner part of the stabilizer core. All the **SOs** on the outermost parts of the assembly are connected to the **JO** by a conductive thermal resistance.

Table 4 also reports the constitutive relations adopted for the heat transfer coefficients and friction factors of the **FOs**. Note that for all the **FOs** the Dittus-Boelter correlation has been adopted for the sake of simplicity, even though the range of Reynolds for the fluid there would possibly require some correlations more suited for the laminar regime. However, this choice has a negligible impact on the assessment of the capability of the tool to model TH transients in such cable.

The simulation is performed heating **SO1** and observing the slug propagation along and across the conductor. Regarding the spatial discretization, 200 elements are used for the simulation of which 50 in the heated (refined) zone, and the time marching proceeds with a constant step of 0.05 s. The computed results for the tested transient are reported in Fig. 14 for the **SOs** components lying on the vertical line reported in Fig. 13a. The heated stack (**SO1**) shows the highest temperature across the conductor, with thermal diffusion at the boundaries of the heated zone, both downstream and upstream. From **SO1**, the heat propagates by conduction across the cable and reaches the opposite side of the cable, where the stabilizer element **SO17** and the tape stack **SO4** increase their temperature simultaneously. The temperature of two **FOs** is also reported: **FO1**, directly in contact with the heated stack, and **FO13**, corresponding to the central channel. The computed temperature for both reveals the heat transport by advection in the downstream direction, at different speeds though. The heat transport by advection allows the pre-heating of the solid components by few tenths of Kelvin downstream of the heated zone, so that the flat temperature profiles at the outlet of the conductor stand at a higher level than the inlet.

The capability of the model to correctly reproduce the symmetrical propagation of the heat across the conductor cross section has been checked, as reported in Fig. 15. The temperature relative difference for the randomly selected couples of **SOs** and **FOs** located symmetrically with respect to the heated **SO1** is almost at the machine precision (10^{-12}), confirming the positive results of Test 2.

4.3. Test 3

For the Test 3, based on a single-core HVDC-HTS cable, the **CO** is assembled as reported in Fig. 16: 1 **SO**, 6 **JOs**, and 2 **FOs** in counter-flow. The **SO** and inner wall of the inner cryostat, which is modeled as a **JO**, are separated by the inlet **FO**, which is thermally connected to both by convection. The two walls of both cryostats, all modeled as **JOs**, interact through radiation. The electrical and thermal insulant, modeled as a single **JO,** is thermally connected by convection with the return **FO**, and by conduction with the outer wall of the inner cryostat. The outer insulation, the outermost **JO**, thermally interacts by conduction with the outer wall of the external cryostat and with the external air at 300.15 K and 0.1 MPa by convection with a given heat transfer coefficient. The main geometrical parameters and features are reported in Table 2 while operational attributes are collected in Table 5.

The **CO** is discretized in space using 200 elements. The steady state operating condition for the conductor at hand is obtained as the arrival point of a transient (time step of 10 s) where the different **SOs** and **JOs** are initially at the temperature of the neighboring fluids (30 K for the SC core and inner shell of the inner cryostat, 100 K for the outer shell of the inner cryostat, the inner insulation and the inner shell of the outer cryostat, respectively) or of the environment (the outer shell of the outer cryostat and the outer insulation). The environmental load is applied throughout the transient to the outer insulation layer, up to stabilization of the temperature at the final steady state. The results are collected in Fig. 17. A wide temperature range is shown along and across the conductor. The two outermost components have a very small temperature variation along the cable, and the average difference between the temperature of the outer insulation and outer shell of the outer cryostat is $\sim$ 0.34 K, enough to allow an integral parasitic power entering the conductor of 8 kW. The parasitic heat is transmitted by radiation to the inner shell and from there it is removed by the gaseous N_2, which drives also the temperature of the inner insulation and the connected outer shell of the inner cryostat from the inlet value of 100 K to $\sim$ 140 K at the outlet (corresponding to the coordinate 0 of the cable, which is set at the inlet of the inner channel). Only a small fraction (<1%) of the integral parasitic heat arrives to the innermost portion of the conductor, where it is removed by the GHe, causing a temperature increase along the SC core of $\sim$ 1 K.

The test of the TDD is passed when the mass conservation law and the first principle of thermodynamic are both satisfied. A focus on the radiative heat transfer mechanism is proposed in Fig. 18 which shows the total power per unit length entering the cable from the external environment, which is then transferred by radiation through the inner and outer surfaces of the **JOs** constituting the outer cryostat. The power per unit length transferred by radiation through the inner cryostat turns out to be about two orders of magnitude lower, due to the high efficiency of the GN_2 thermal shield.

5. Open-source project and perspectives

The OPENSC^2 software has been developed to provide an accessible tool to analyze the thermal–hydraulic transients in superconducting cables for energy applications. The robustness of the implemented methods has been demonstrated through a Test-Driven Development, performing rigorous benchmarks whenever possible, which allowed analyzing case studies relative to very different cable topologies and applications.

OPENSC^2 is open-source and is made available to the community under the AGPL v3 (Affero General Public License 3.0) or any other version of it on the GitHub repository OPENSC2 (https://github.com/MAHTEP/OPENSC2) and associated to a DOI (https://doi.org/10.5281/zenodo.6409285) via the Zenodo open repository. In that sense, it is accessible to anybody willing to use it and to modify it, including the possibility to further open-source development by colleagues from other institution. On top of the transparency of the models

and algorithms implemented in the tool, the open-source release will enable researchers to customize the tool according to their specific needs and independently verify the design of cables and magnets that, as far as the fusion field is concerned for instance, are very often carried out with public money and could then be subject to public reviews and checks.

The future development of OPENSC2 targets the multi-physics simultaneous analysis of the current distribution within the cables, that could trigger thermal–hydraulic transients due, for instance, to the onset of AC losses, up to the loss or lack of capability to accomplish the operating function. As far as the numerical aspects are concerned, the actual static grid and uniform time stepping will be enriched with adaptivity both in space and time, to allow a more accurate solutions where steep spatial gradients are localized and when a fast variation of the solution is detected. The tool, which is currently not parallelized nor optimized in any sense, will also undergo an analysis to identify possible optimization strategies for the solution algorithms.

CRediT authorship contribution statement

Laura Savoldi: Conceptualization, Methodology, Formal analysis, Investigation, Validation, Resources, Supervision, Writing – original draft. **Daniele Placido:** Methodology, Software, Formal analysis, Data curation, Investigation, Visualization, Writing – review & editing. **Sofia Viarengo:** Methodology, Investigation, Visualization, Writing – review & editing.

Declaration of Competing Interest

The authors declare that they have no known competing financial interests or personal relationships that could have appeared to influence the work reported in this paper.

Acknowledgements

The authors are grateful to R. Deias who helped in running the code and passing the Tests 2 and 3, and to F. Freschi for support and useful discussion.

References

[1] Rossi L. Superconductivity: Its role, its success and its setbacks in the LARGE HADRON COLlider of CERN. Supercond Sci Technol 2010;23(3):034001.
[2] Bruzzone P. Superconductivity and fusion energy - The inseparable companions. Supercond Sci Technol 2015;28(2):024001.
[3] Jones H. Superconductors in the transmission of electricity and networks. Energy Policy 2008;36(12):4342–5.
[4] Alonso JR, Antaya TA. Superconductivity in Medicine. Http://DxDoiOrg/101142/S1793626812300095 2013;05:227–63. Doi: 10.1142/S1793626812300095.
[5] Shrivastava SK. Applications of superconductivity in electric power and transportation system. JES Publ 2020;11:8.
[6] Zhou XS, Lu B, Ma YJ. A Review on Superconducting Magnetic Energy Storage. Adv Mater Res 2013;614–615:825–8. https://doi.org/10.4028/WWW.SCIENTIFIC.NET/AMR.614-615.825.
[7] Barzi E, Zlobin A V. Nb<Subscript>3</Subscript>Sn Wires and Cables for High-Field Accelerator Magnets. In: Schoerling, D. Zlobin A, editor. Nb3Sn Accel. Magnets. Part. Accel. Detect., Springer, Cham; 2019, p. 23–51. Doi: 10.1007/978-3-030-16118-7_2.
[8] Rossi L, Senatore C. HTS Accelerator Magnet and Conductor Development in Europe. Instruments 2021, Vol 5, Page 8 2021;5:8. Doi: 10.3390/INSTRUMENTS5010008.
[9] Horvath A, Rachlew E. Nuclear power in the 21st century: Challenges and possibilities. Ambio 2016;45(S1):38–49.
[10] Adelerhof J, Thoopal MB, Lee D, Hardy C. Clean and sustainable fusion energy for the future. PAM Rev Energy Sci Technol 2015;1:20–42.
[11] Johnson JL. Stellarator and heliotron devices. Nucl Fusion 1999;39(2):293–4.
[12] Wanner M, Feist J-H, Renner H, Sapper J, Schauer F, Schneider H, et al. Design and construction of WENDELSTEIN 7-X. Fusion Eng Des 2001;56-57:155–62.
[13] Wolf RC, Beidler CD, Dinklage A, Helander P, Laqua HP, Schauer F, et al. Wendelstein 7-X program - demonstration of a stellarator option for fusion energy. IEEE Trans Plasma Sci 2016;44(9):1466–71.
[14] Fujiwara M, Kawahata K, Ohyabu N, Kaneko O, Komori A, Yamada H, et al. Overview of LHD experiments. Nucl Fusion 2001;41(10):1355–67.
[15] Iiyoshi A, Komori A, Ejiri A, Emoto M, Funaba H, Goto M, et al. Overview of the large helical device project. Nucl Fusion 1999;39(9Y):1245–56.
[16] Rummel T, Ribe K, Ehrke G, Rummel K, John A, Monnich T, et al. The superconducting magnet system of the stellarator wendelstein 7-X. IEEE Trans Plasma Sci 2012;40(3):769–76.
[17] Warmer F, Beidler CD, Dinklage A, Wolf R. From W7-X to a HELIAS fusion power plant: Motivation and options for an intermediate-step burning-plasma stellarator. Plasma Phys Control Fusion 2016;58(7):074006.
[18] Queral V, Volpe FA, Spong D, Cabrera S, Tabarés F. Initial exploration of high-field pulsed stellarator approach to ignition experiments. J Fusion Energy 2018;37(6):275–90.
[19] Mitchell N, Zheng J, Vorpahl C, Corato V, Sanabria C, Segal M, et al. Superconductors for fusion: a roadmap. Supercond Sci Technol 2021;34(10):103001.
[20] Holtkamp N. An overview of the ITER project. Fusion Eng Des 2007;82(5-14):427–34.
[21] Fiore K. Nuclear energy and sustainability: Understanding ITER. Energy Policy 2006;34(17):3334–41.
[22] Llewellyn Smith C, Ward D. Fusion. Energy Policy 2008;36(12):4331–4.
[23] Song YT, Wu ST, Li JG, Wan BN, Wan YX, Fu P, et al. Concept design of CFETR tokamak machine. IEEE Trans Plasma Sci 2014;42(3):503–9.
[24] Wan Y, Li J, Liu Y, Wang X, Chan V, Chen C, et al. Overview of the present progress and activities on the CFETR. Nucl Fusion 2017;57(10):102009.
[25] Muzzi L, De Marzi G, Di Zenobio A, Della Corte A. Cable-in-conduit conductors: Lessons from the recent past for future developments with low and high temperature superconductors. Supercond Sci Technol 2015;28(5):053001.
[26] Donné T. European research roadmap to the realisation of fusion energy. EUROfusion 2018.
[27] Sedlak K, Anvar VA, Bagrets N, Biancolini ME, Bonifetto R, Bonne F, et al. Advance in the conceptual design of the European DEMO magnet system. Supercond Sci Technol 2020;33(4):044013.
[28] Tobita K, Hiwatari R, Utoh H, Miyoshi Y, Asakura N, Sakamoto Y, et al. Overview of the DEMO conceptual design activity in Japan. Fusion Eng Des 2018;136:1024–31.
[29] Kim K, Im K, Kim HC, Oh S, Park JS, Kwon S, et al. Design concept of K-DEMO for near-term implementation. Nucl Fusion 2015;55(5):053027.
[30] Kim HW, Im K, Lee HJ, Kim H-T, Kwon S, Brown T, et al. Design updates of magnet system for Korean fusion demonstration reactor. K-DEMO Fusion Eng Des 2019;146:1086–90.
[31] Sorbom BN, Ball J, Palmer TR, Mangiarotti FJ, Sierchio JM, Bonoli P, et al. ARC: A compact, high-field, fusion nuclear science facility and demonstration power plant with demountable magnets. Fusion Eng Des 2015;100:378–405.
[32] Whyte DG, Minervini J, LaBombard B, Marmar E, Bromberg L, Greenwald M. Smaller & sooner: exploiting high magnetic fields from new superconductors for a more attractive fusion energy development path. J Fusion Energy 2016. https://doi.org/10.1007/s10894-015-0050-1.
[33] Whyte D. Small, modular and economically attractive fusion enabled by high temperature superconductors. Philos Trans R Soc A Math Phys Eng Sci 2019;377(2141):20180354.
[34] Tsunematsu T. Broader Approach to fusion energy. Fusion Eng Des 2009;84(2-6):122–4.
[35] Ambrosino R. DTT - Divertor Tokamak Test facility: A testbed for DEMO. Fusion Eng Des 2021;167:112330. https://doi.org/10.1016/J.FUSENGDES.2021.112330.
[36] Barabaschi P, Kamada Y, Shirai H. Progress of the JT-60SA project. Nucl Fusion 2019;59(11):112005.
[37] Pizzuto A, Semeraro L, Zani L, Bayetti P, Cucchiaro A, Decool P, et al. JT-60SA toroidal field magnet system. IEEE Trans Appl Supercond 2008;18(2):505–8.
[38] Di Zenobio A. DTT: a challenging framework for a sound superconducting magnets design. Magn Technol Conf 2021.
[39] Thomas H, Marian A, Chervyakov A, Stückrad S, Salmieri D, Rubbia C. Superconducting transmission lines - Sustainable electric energy transfer with higher public acceptance? Renew Sustain Energy Rev 2016;55:59–72. https://doi.org/10.1016/j.rser.2015.10.041.
[40] Stemmle M, Merschel F, Noe M, Hobl A. Ampacity project - Worldwide first superconducting cable and fault current limiter installation in a German city center. IET Conf Publ 2013, 2013. https://doi.org/10.1049/cp.2013.0905.
[41] Li J, Zhang L, Ye X, Xia F, Cao Y. Demonstration Project of 35 kV/1 kA Cold Dielectric High Temperature Superconducting Cable System in Tianjin. IEEE Trans Appl Supercond 2020;30(2):1–5.
[42] Sytnikov VE, Bemert SE, Kopylov SI, Romashov MA, Ryabin TV, Shakaryan YG, et al. Status of HTS cable link project for St. Petersburg Grid. IEEE Trans Appl Supercond 2015;25(3):1–4.
[43] Yumura H, Ashibe Y, Ohya M, Itoh H, Watanabe M, Masuda T, et al. Update of YOKOHAMA HTS cable project. IEEE Trans Appl Supercond 2013;23(3):5402306.
[44] Savoldi L, Placido D, Viarengo S. Thermal-hydraulic models the HTS power-transmission cables: status and needs. Superconductor Science and Technology 2022;35(044001):4. https://doi.org/10.1088/1361-6668/ac4f3c.
[45] Open Science | European Commission n.d. https://ec.europa.eu/info/research-and-innovation/strategy/strategy-2020-2024/our-digital-future/open-science_en (accessed July 9, 2021).
[46] Bottura L. Thermal, Hydraulic, and Electromagnetic Modeling of Superconducting Magnet Systems. IEEE Trans Appl Supercond 2016;26(3):1–7.
[47] Amoskov V, Belov A, Belyakov V, Filatov O, Ilyasov O, Kalinin V, et al. Validation of VINCENTA modelling based on an experiment with the central solenoid model coil of the international thermonuclear experimental reactor. Plasma Devices Oper 2006;14(1):47–59.

[48] Savoldi Richard L, Casella F, Fiori B, Zanino R. The 4C code for the cryogenic circuit conductor and coil modeling in ITER. Cryogenics (Guildf) 2010;50(3):167–76.
[49] Bottura L. A numerical model for the simulation of quench in the ITER magnets. J Comput Phys 1996;125:26–41. https://doi.org/10.1006/JCPH.1996.0077.
[50] Lewandowska M, Dembkowska A, Heller R, Wolf M. Thermal-hydraulic analysis of an HTS DEMO TF coil. Cryogenics (Guildf) 2018;96:125–32.
[51] Zappatore A, Fietz WH, Heller R, Savoldi L, Wolf MJ, Zanino R. A critical assessment of thermal–hydraulic modeling of HTS twisted-stacked-tape cable conductors for fusion applications. Supercond Sci Technol 2019;32(8):084004.
[52] Savoldi L, Zanino R. M & M: Multi-conductor Mithrandir code for the simulation of thermal-hydraulic transients in superconducting magnets. Cryogenics (Guildf) 2000. https://doi.org/10.1016/S0011-2275(00)00027-8.
[53] Zanino R, Santagati P, Savoldi L, Marinucci C. Joint+conductor thermal-hydraulic experiment and analysis on the Full Size Joint Sample using MITHRANDIR 2.1. IEEE Trans Appl Supercond 2000. https://doi.org/10.1109/77.828427.
[54] Zanino R, Richard LS. Multiscale approach and role of validation in the thermal-hydraulic modeling of the ITER superconducting magnets. IEEE Trans Appl Supercond 2013;23(3):4900607.
[55] Nicollet S, Bessette D, Ciazynski D, Duchateau JL, Lacroix B. Cross checking of Gandalf and Vincenta on the CS behaviour during ITER reference scenario. AIP Conf Proc 2010. https://doi.org/10.1063/1.3422315.
[56] Beck K. Test-Driven Development: By Examples. Addison-Wesley Professional; 2002.
[57] Zappatore A, Heller R, Savoldi L, Wolf MJ, Zanino R. A new model for the analysis of quench in HTS cable-in-conduit conductors based on the twisted-stacked-tape cable concept for fusion applications. Supercond Sci Technol 2020;33(6):065004.
[58] Zappatore A, Augieri A, Bonifetto R, Celentano G, Savoldi L, Vannozzi A, et al. Modeling Quench Propagation in the ENEA HTS Cable-In-Conduit Conductor. IEEE Trans Appl Supercond 2020;30(8):1–7.
[59] Bruzek CE, Ballarino A, Escamez G, Giannelli S, Grilli F, Lesur F, et al. Cable conductor design for the high-power MgB2 DC superconducting cable project of BEST PATHS. IEEE Trans Appl Supercond 2017;27(4):1–5.
[60] Viarengo S, Freschi F, Placido D, Savoldi L. Current distribution modeling in the open-source OPENSC2 tool for the multi-physics analysis of HTS and LTS superconducting cable. IEEE Transaction on Applied Superconductivity 2022. https://doi.org/10.1109/TASC.2022.3158309.
[61] Zanino R, De Palo S, Bottura L. A two-fluid code for the thermohydraulic transient analysis of CICC superconducting magnets. J Fusion Energy 1995;14(1):25–40.
[62] Placido D, De Marzi G, Di Zenobio A, Ramogida G, Savoldi L. Evaluation of the thermal performance of the SC Feeders for the magnetic system of the Divertor Tokamak Test facility. IEEE Transactions on Applied Superconductivity 2022. https://doi.org/10.1109/TASC.2022.3161249.
[63] Bottura L, Rosso C, Breschi M. A general model for thermal, hydraulic and electric analysis of superconducting cables. Cryogenics (Guildf) 2000;40:617–26. https://doi.org/10.1016/S0011-2275(01)00019-4.
[64] Bottura L, Bottura L. A numerical model for the simulation of quench in the ITER magnets. JCoPh 1996;125:26–41. https://doi.org/10.1006/JCPH.1996.0077.
[65] Zanino R, De Palo S, Bottura L. A two-fluid code for the thermohydraulic transient analysis of CICC superconducting magnets. Undefined 1995;14:25–40. https://doi.org/10.1007/BF02214031.
[66] Magnet system Alphysica n.d. http://www.alphysica.com/venecia.php (accessed November 11, 2021).
[67] Richard LS, Bagnasco M, Zanino R. Multi-solid multi-channel Mithrandir (M3) code for thermal-hydraulic modelling of ITER Cable-in-Conduit Superconductors. Fusion Eng Des 2007;82:1607–13. https://doi.org/10.1016/J.FUSENGDES.2007.04.035.